TGF-β in BM sections fixed with dry ice-cold ethanol. LAP was detected in various cells, including scattered megakaryocytes, well known to produce latent TGF-β abundantly (Figure 2A), whereas distribution of active TGF-β was highly restricted to a minor population of LAP-positive cells that formed long, spindled structures distinct from VE-cadherin-positive blood vessels (Figures 2B and 2C). Of particular note, megakaryocytes became reactive to anti-TGFβ antibody only after citric acid treatment (Figure S2C). These findings indicated that the fixation of BM sections with ethanol alone does not activate latent TGF-β and further supported the specificity of anti-TGFβ antibody.

Latent forms of TGF-β accumulate in the ECM through direct binding between the LTBP and ECM (Annes et al., 2003). Although the precise mechanism of activation of latent TGF-β is not clear, the integrins αvβ6 and αvβ8 most likely facilitate proteolytic degradation of LAP by matrix metalloproteinases (Annes et al., 2003, 2004; Munger et al., 1999; Mu et al., 2002). In this regard integrin function is tightly linked with proteolytic processes. LTBP was expressed in both long, spindled cells and megakaryocytes (Figure S2D), indicating that these cells produce abundant latent TGF-β. In contrast, integrin-β8 (*Itgb8*) was specifically expressed by the long, spindled-cell structure that marked abundantly for active TGF-β (Figure 2D), whereas integrin-β6 expression was not detected in any BM stromal or hematopoietic cells (data not shown).

BM Glial Cells Produce Active TGF-β

The aforementioned findings led us to identify BM cell types that express *Itgb8*. RT-PCR analysis revealed that hematopoietic cells and BM stromal cells did not express *Itgb8* at all (Figure S3A). We then focused on GFAP-positive glial cells because Schwann cells reportedly express *Itgb8* (Figure S3A) (Cambier et al., 2005; Chernousov and Carey, 2003). Schwann cells of neural crest origin in the peripheral nervous system are the counterparts of astrocytes in the central nervous system. There are two types of Schwann cells: myelinating and nonmyelinating. Myelinating Schwann cells, which provide the neural myelin sheath, express myelin basic protein (MBP), but not GFAP. In contrast, nonmyelinating Schwann cells, which ensheath several small axons, express GFAP, but not MBP. Myelination occurs for large axons 1–25 μm in diameter, whereas most postganglionic autonomic axons are less than 1 μm in diameter and are unmyelinated (Jessen and Mirsky, 2005). To learn if the cells of interest were glial cells, we analyzed the expression in BM of GFAP, a glial cell-specific member of the intermediate filament family (Coulombe and Wong, 2004). First, we characterized BM GFAP-positive cells in detail using *GFAP* promoter-driven GFP (GFAP-GFP) transgenic mice (Suzuki et al., 2003). The vast majority of GFP-positive cells stained for active TGF-β (Figure 3A) and expressed *Itgb8* and S100β, a marker antigen for glial cells (Figures S3B and S3C). These cells were much smaller in diameter than other peripheral nerve cells, but the size and appearance of these GFAP-positive cells were very similar to those described for Schwann cells in the BM (Calvo and Forteza-Vila, 1970). To confirm that these GFAP-positive cells were nonmyelinating Schwann cells, we examined them using a confocal laser microscope under high magnification. As shown in Figure 3B, GFAP-positive cells were present in parallel with neurofilament (NF)-positive axons. Analysis of transverse sections revealed that GFAP-positive cells ensheathed NF- and tyrosine hydroxylase (TH)-positive axons (Figures 3C–3E). Immunostaining of transverse sections confirmed that these GFAP-positive cells were positive for both active TGF-β and *Itgb8* (Figures 3F and 3G). Additional costaining with anti-VE-cadherin and anti-GFAP or anti-*Itgb8* antibodies revealed that the VE-cadherin-positive endothelial cells and GFAP- and *Itgb8*-positive cells of interest were distinct and lay in parallel in close proximity (Figure S4; Movie S1). These results strongly suggested that the cells that play a role in HSC hibernation were nonmyelinating Schwann cells.

Mendez-Ferrer et al. recently reported that nestin-positive MSCs are a component of the BM niche (Méndez-Ferrer et al., 2010). Nestin is an intermediate filament expressed in various cell types, including cells of the central and peripheral nervous system and neural crest derivatives (Guérette et al., 2007). Using an antibody against PDGFRα, a marker antigen for MSCs (Morikawa et al., 2009; Omatsu et al., 2010), we combined immunohistochemical and ArrayScan analyses to understand the relationship between GFAP-positive glial cells and MSCs. PDGFRα-positive cells, nestin-positive cells, and GFAP-positive cells represented 0.05%, 0.026%, and 0.004% of BM area, respectively (Figure S5A). Of particular interest was that all GFAP-positive cells were positive for nestin (Figures S5B and S5C) but negative for PDGFRα (Figures S5B and S5D) and that PDGFRα-positive MSCs were not positive for active TGF-β (Figure S5E). PDGFRα-positive MSCs and nestin-positive cells largely overlapped but showed different distributions as well (Figures S5B and S5F). These findings indicate that GFAP-positive cells and PDGFRα-positive MSCs were distinct. Expression of smooth muscle actin, a marker of pericytes, was also lacking in GFAP-positive cells (data not shown). Therefore, we concluded that nonmyelinating Schwann cells distinct from PDGFRα$^+$ MSCs are the cells responsible for production of active TGF-β.

A Significant Proportion of HSCs Exists in Contact with Glial Cells

BM glial cells that produce *Itgb8*, which activates, TGF-β are attractive candidates for BM niche cells. To determine whether glial cells are in contact with HSCs in BM, we stained BM sections with antibodies against CD150, CD48, CD41, and

(E) Phosphorylation levels of Smad2/3 in *Tgfbr2*-deficient HSCs. CD34$^-$KSL HSCs were purified from *Tgfbr2*$^{+/+}$*Rag2*$^{-/-}$ and *Tgfbr2*$^{del/-}$*Rag2*$^{-/-}$ BM at 2 weeks after pIpC treatment, stained with anti-p-Smad2/3 antibody, and automatically assayed by ArrayScan. As a negative control, *Tgfbr2*$^{+/+}$*Rag2*$^{-/-}$ HSCs were similarly stained with rabbit IgG control antibody. Data from two independent experiments were pooled.

(F) Cell cycle status of *Tgfbr2*-deficient HSCs. At 2 weeks after pIpC treatment, mice were given BrdU-containing water for 7 days. After administration of BrdU to mice for 7 days, CD34$^-$KSL HSCs were purified from *Tgfbr2*$^{+/-}$*Rag2*$^{-/-}$ and *Tgfbr2*$^{del/-}$*Rag2*$^{-/-}$ BM cells, stained with an anti-BrdU antibody, and then analyzed for BrdU uptake by ArrayScan (n = 5). Error bar represents SEM. $^{**}p < 0.001$.

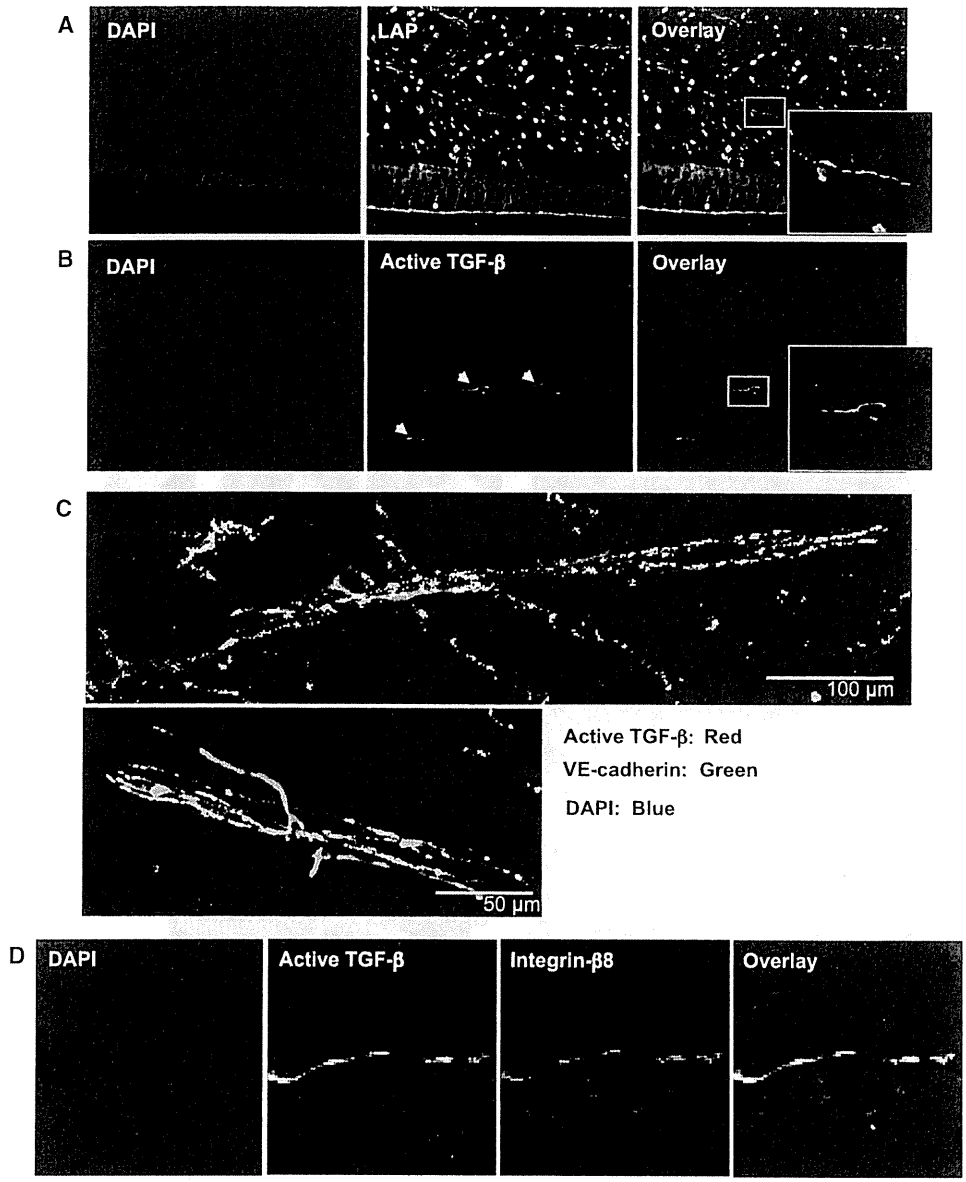

Figure 2. A Specialized Cell Type Produces Active TGF-β in BM

(A) Distribution of latent TGF-β in BM. BM sections were stained with DAPI (blue) and anti-LAP antibody (green). A magnified image of the boxed cell is depicted in the inset.

(B) Distribution of active TGF-β in BM. BM sections were stained with DAPI (blue) and anti-TGF-β antibody (green). A magnified image of the boxed cell is depicted in the inset. Arrowheads indicate active TGF-β-positive endothelial cell-like spindle cells (arrowheads).

(C) Costaining of BM with anti-TGF-β and anti-VE-cadherin antibodies. BM sections were stained with DAPI (blue), anti-TGF-β antibody (red), and anti-VE-cadherin antibody (green).

(D) Costaining of BM with anti-TGF-β and anti-*Itgb8* antibodies. BM sections were stained with DAPI (blue), anti-TGF-β antibody (green), and anti-*Itgb8* antibody (red). All data were obtained by ArrayScan.

See also Figures S2 and S3.

lineage markers to identify HSCs as well as simultaneously staining BM sections with antibodies against GFAP, osteocalcin, and VE-cadherin. We then evaluated these sections quantitatively by ArrayScan to determine the positional relationships between HSCs and BM glial cells (Figure 4A). GFAP-expressing glial cells were in direct contact with 23.3% ± 5.4% of $CD150^{+}CD48^{-}CD41^{-}Lin^{-}$ HSCs (Figures 4B and 4C), whereas 13.3% ± 4.2% and 30.7% ± 3.7% of HSCs were in contact, respectively, with osteocalcin-expressing osteoblastic cells and VE-cadherin expressing vascular cells (Figures 4B, 4D, and 4E). Although 32.7% ± 5.7% of HSCs lay apart from these cells (Figure 4B), this may reflect our failure to detect HSC

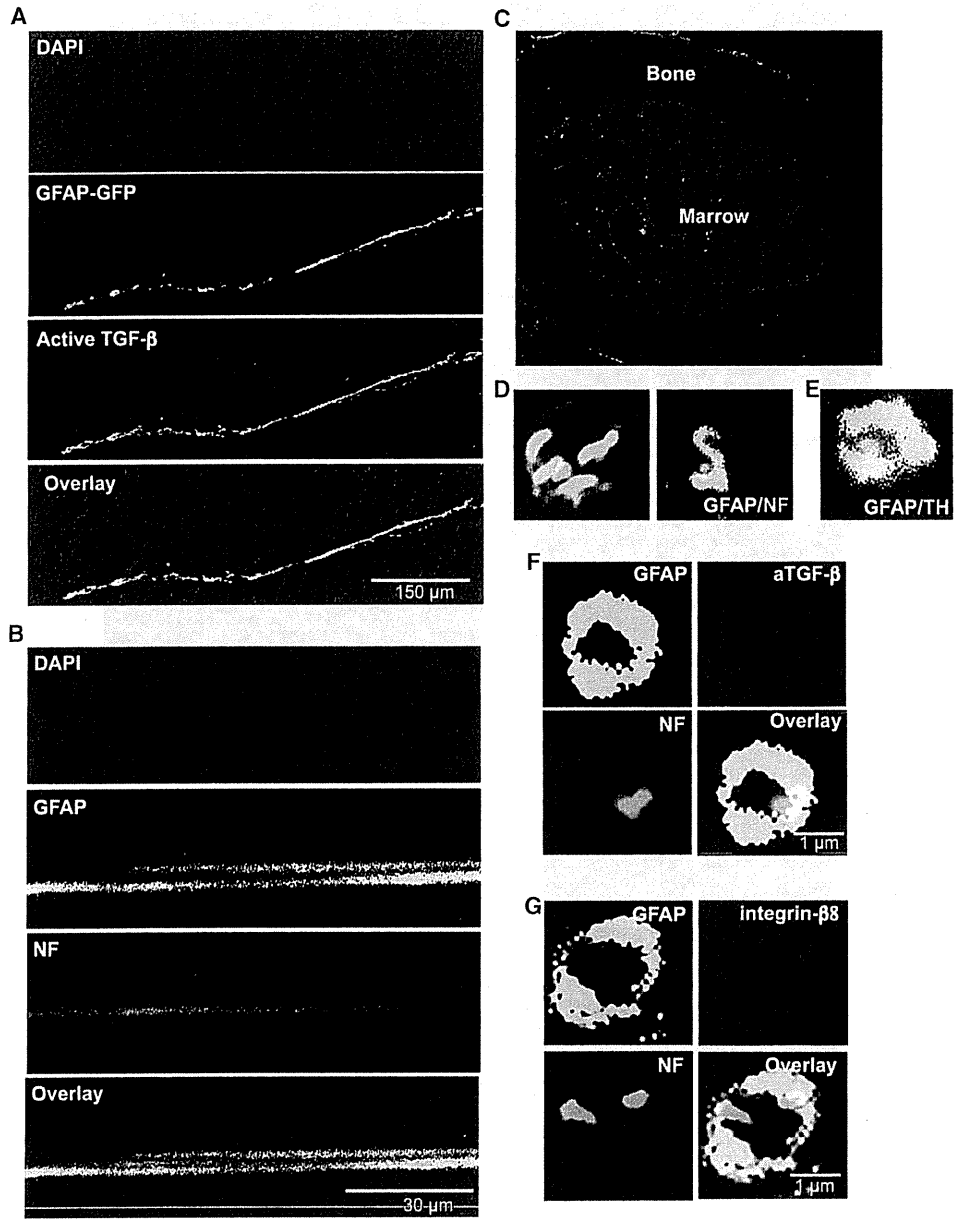

Figure 3. GFAP-Positive Cells Activate Latent TGF-β

(A) Expression of active TGF-β in GFAP-positive cells in BM. BM sections from *GFAP*-promoter-driven GFP transgenic mice (GFAP-GFP) were stained with DAPI (blue) and anti-TGF-β antibody (red), and immunofluorescence signals were overlaid with that of GFP. Representative magnified overlay images are presented.

(B) Longitudinal sections of GFAP-GFP transgenic mouse BM stained with anti-NF antibody (red). Representative magnified overlay images are presented.

(C–E) Cross sections of GFAP-GFP transgenic mouse BM. Unstained, low-magnification image (C) and cross sections of GFAP-GFP transgenic mouse BM stained with anti-NF antibody (D) or with anti-TH antibody (red) (E) with higher magnification are shown.

(F and G) Cross sections of GFAP-GFP transgenic mouse BM stained with anti-TGF-β antibody or anti-*Itgb8* antibody and with anti-NF antibody.

See also Figures S3, S4, and S5, and Movie S1.

contact in 2-dimensional BM section scans. Alternatively, HSCs may have been in contact with as yet unidentified cells. Of particular interest is that $CD34^{+}KSL$ progenitor cells lay apart from glial cells (data not shown). Furthermore, GFAP-expressing glial cells were not detected in fetal livers, in which developing HSCs are in the cell cycle as their numbers expand (Morrison et al., 1995).

Glial cells have never been examined for a niche cell-like capacity to support HSCs. Although BM cells enriched in Schwann cells could not be prepared, Schwann cells prepared from sciatic nerves expressed *Tgfb1*, *Tgfb2*, and *Tgfb3* as well as *Itgb8*. Surprisingly, they also expressed major HSC niche factor genes, including *Cxcl12*, *c-kit ligand* (*kitl*), *anginpoitin-1* (*Angpt1*), and *Tpo* (Figure S6).

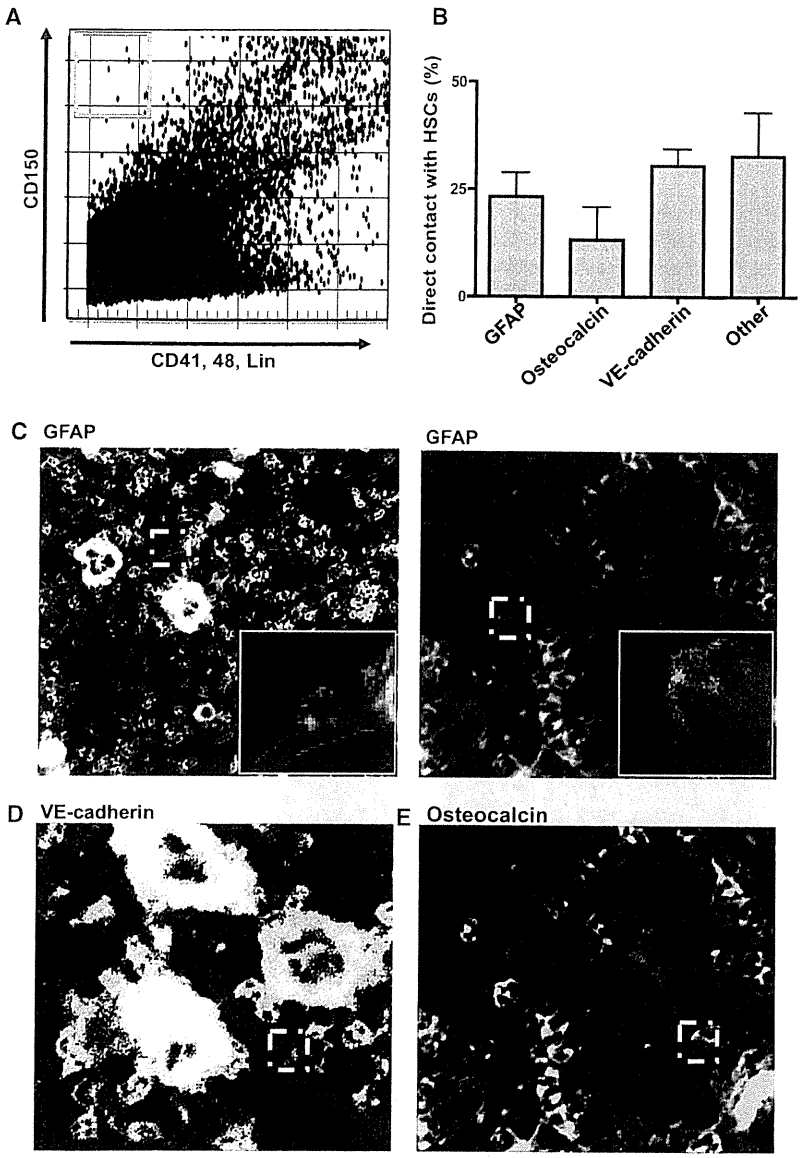

Figure 4. HSCs Exist in Contact with Glial Cells in BM

(A) Two-dimensional presentation of wild-type BM section data automatically acquired by ArrayScan. Frozen BM sections were stained with antibodies against CD150 (red), CD48, CD41, and lineage markers (green), and GFAP (blue). Gated cells in a red square represent $CD150^{+}CD48^{-}CD41^{-}Lin^{-}$ HSCs.

(B) Positional relationship of HSCs with niche cells. Data from whole BM sections imaged by ArrayScan were analyzed in terms of the positional relationship of HSCs with niche cells, including osteocalcin-positive osteoblastic niche cells and VE-cadherin-positive vascular niche cells together with GFAP-positive glial cells. Frozen wild-type BM sections were stained with anti-CD150 (red), anti-CD48, -CD41, and -lineage markers (green), and anti-GFAP (blue) antibodies. ArrayScan data from whole BM sections were analyzed for positional relationships between HSCs and known niche cells (n = 10). Error bar represents SD.

(C) Representative fluorescence micrographs of colocalizing HSCs (boxed in A) with GFAP-positive glial cells. Frozen wild-type BM sections were stained with antibodies against CD150 (red), against CD48, CD41, and lineage markers (green), and against GFAP (blue). Magnified images are shown in the insets.

(D and E) Representative fluorescence images of HSCs colocalizing with VE-cadherin-positive vascular niche cells (D) and osteocalcin-positive osteoblastic niche cells (E) (boxed). Frozen wild-type BM sections were stained with antibodies against CD150 (red), against CD48, CD41, and lineage markers (green), and against VE-cadherin or osteocalcin (blue).

See also Figures S1 and S6.

Denervation of Sympathetic Nerve Results in Loss of HSCs

To provide direct evidence that BM Schwann cells are a component of the BM niche and were responsible for the maintenance of HSCs' hibernation state, we attempted to delete ensheathing glial cells in BM via Wallerian degeneration by transecting postganglionic sympathetic nerves directly (Fernando et al., 2002). Although denervation of sciatic myelinated motor axons was reported to induce proliferation of myelinating Schwann cells (Murinson and Griffin, 2004), other studies indicated that Schwann cells undergo prompt apoptotic cell death in the nerve distal to axotomy both in neonates (Grinspan et al., 1996) and in adult rodents (Sulaiman et al., 2002). Nerve injury reduces neuregulin-1 signaling and leads to apoptosis of Schwann cells (D'Antonio et al., 2006). Based on the assumption that similar loss of nonmyelinating Schwann cells by apoptosis would occur, the lumbar sympathetic trunk was cut unilaterally at the level of L2, L3, and L4 to denervate sympathetic nerves to the biceps femoris muscle and the BM, with a sham operation performed contralaterally. This surgical procedure spared motor and sensory nerves, leaving the animal's motion intact (Noguchi et al., 1999), and resulted in significant decreases in the number of GFAP-positive cells as well as of active TGF-β-positive cells (Figure 5A). Loss of GFAP-positive cells was also confirmed by S100β staining (data not shown). Although total BM cells did not differ significantly in number between left and right femora (data not shown), loss of HSCs on the denervated side was manifested as early as day 3 after surgery, and HSC numbers fell to one-fifth of those in contralateral BM by day 7 (Figures 5B and 5C). Although we cannot exclude the possibility that sympathetic denervation induces secondary injury, we confirmed that the integrity of other BM niche components such as VE-cadherin-positive endothelial cells, PDGFRα-positive MSCs, and osteocalcin-positive osteoblasts remained intact at 1 week after denervation (Figure 5D).

To confirm the loss of HSCs after denervation, we performed competitive repopulation analyses using BM cells harvested 1 month after sympathetic nerve transfection. One million cells from denervated or contralateral BM were transplanted into

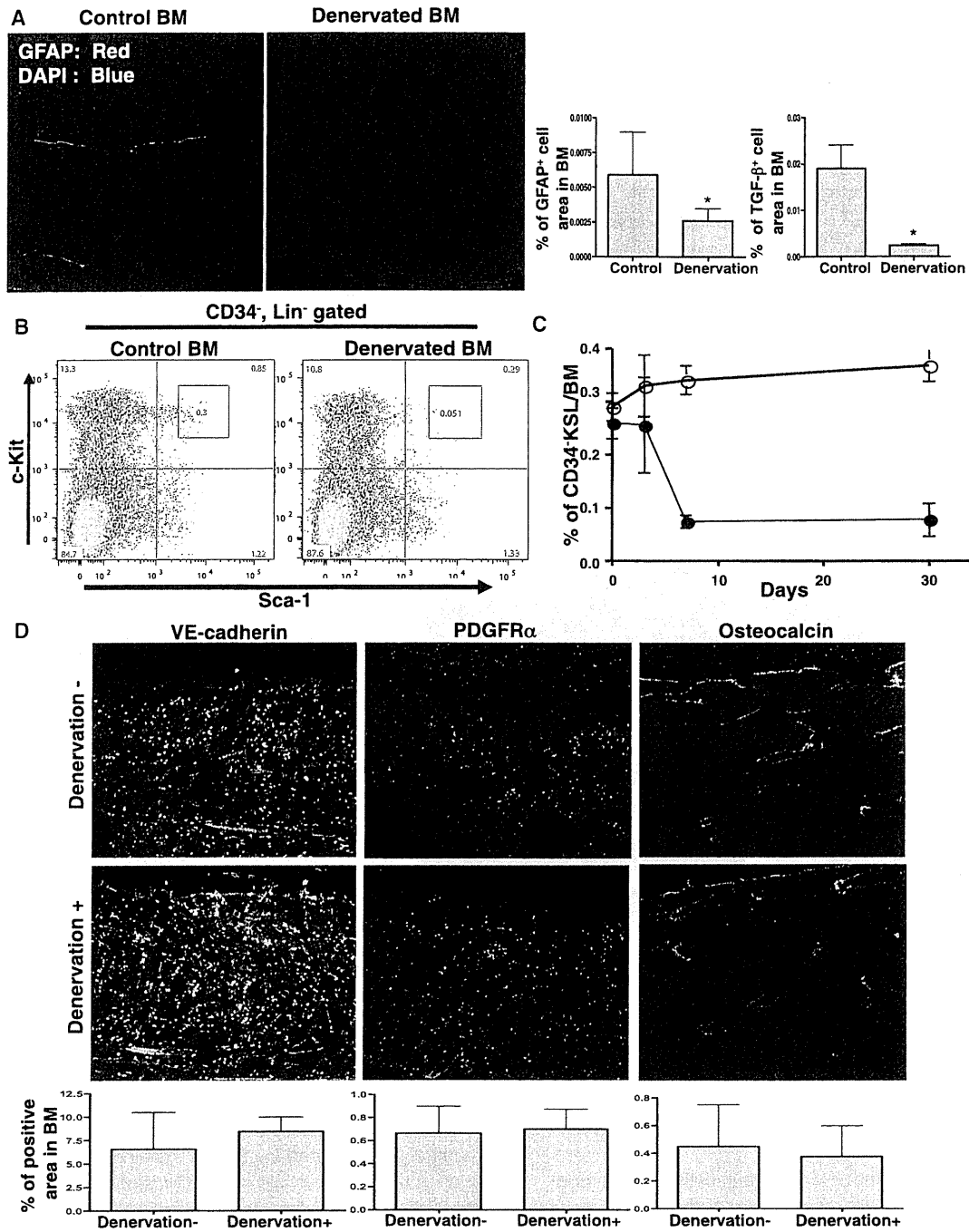

Figure 5. Denervation of Sympathetic Nerve Results in Loss of HSCs

(A) Distribution of GFAP-positive and active TGF-β-positive cells in BM after sympathetic nerve denervation. BM sections were stained with DAPI (blue) and with anti-GFAP antibody (red, left panels) or anti-TGF-β antibody (data not shown). Control sections were obtained from contralateral sham-operated BM. Right panels demonstrate results of quantitative analysis of fluorescence-positive area for GFAP or TGF-β in BM section by ArrayScan software (n = 10). Error bar represents SEM. *p < 0.01.

(B) Frequencies of c-Kit$^+$Sca-1$^+$ cells in CD34$^-$Lin$^-$ cells in control and denervated BM.

(C) Time course analysis of frequencies of CD34$^-$KSL HSCs in control and denervated BM. Frequencies of CD34$^-$KSL/BM cells are depicted. Data are presented as mean ± SD (n = 4).

(D) Distribution of VE-cadherin-, PDGFRα-, and osteocalcin-positive niche cells in BM after autonomic nerve denervation. BM sections were stained with DAPI (blue) and with anti-VE-cadherin antibody, anti-PDGFRα antibody, or anti-osteocalcin antibody (green). Control sections were obtained from contralateral, sham-operated BM. Lower panels demonstrate results of quantitative analysis of fluorescence-positive areas for VE-cadherin, PDGFRα, or osteocalcin in BM sections, as determined by ArrayScan software (n = 10). Error bar represents SEM. No statistically significant difference between control and denervated BM was demonstrated.

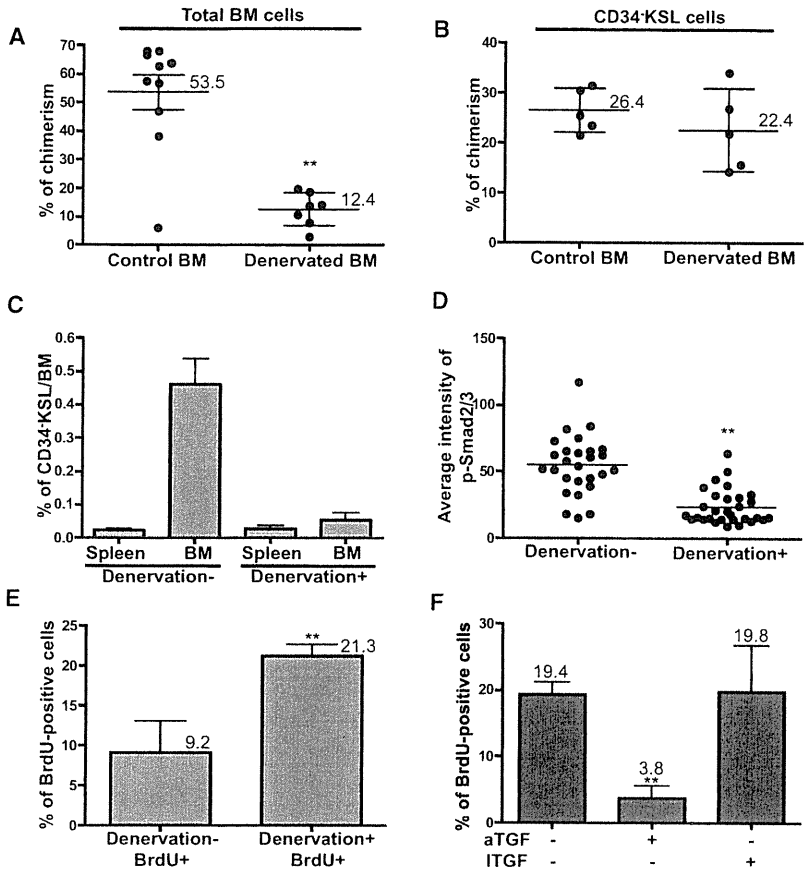

Figure 6. Sympathetic Nerve Denervation Compromises Dormancy of HSCs

(A) Results of long-term competitive repopulation analysis. One million BM cells 1 month after denervation were transplanted into lethally irradiated mice together with 1 × 10^6 total BM competitor cells. Four months later, donor chimerism in PB was determined by FACS. Sham-operated contralateral BM cells were used as controls. Data are presented as mean ± SD (n = 10). **p < 0. 001.

(B) Capacity of purified $CD34^-KSL$ HSCs for long-term repopulation and hematopoiesis. Forty purified $CD34^-KSL$ HSCs 1 month after denervation were transplanted into lethally irradiated mice together with 1 × 10^6 total BM competitor cells. Four months later, donor chimerism in PB was determined by FACS. $CD34^-KSL$ HSCs from sham-operated contralateral BM cells were used as controls. Data are presented as mean ± SD (n = 5).

(C) Frequencies of $CD34^-KSL$/BM cells in control and BM-denervated mouse BM and spleen 1 week after denervation. Data are presented as mean ± SD (n = 5).

(D) Phosphorylation levels of Smad2/3 in HSCs after selective denervation. $CD34^-KSL$ HSCs were purified from control and denervated BM at day 7 after denervation, stained with anti-p-Smad2/3 antibody, and assayed by ArrayScan. **p < 0. 001.

(E) Cell cycle status of HSCs in denervated BM. One week after denervation, mice were fed with BrdU-containing water for 7 days, then $CD34^-KSL$ HSCs were isolated from control or denervated BM, stained with anti-BrdU antibody, and analyzed by ArrayScan. Data are presented as mean ± SD (n = 3). **p < 0. 001.

(F) Restoration of HSC dormancy by infusion of active TGF-β. One week after denervation, administration of either latent or active TGF-β (ITGF and aTGF, respectively) began, infused intraperitoneally into mice every other day at a dose of 40 μg/kg. BrdU in drinking water also was begun. Intraperitoneal infusions and BrdU administration both were given for 1 week. At day 14 after denervation, $CD34^-KSL$ HSCs were isolated, stained with anti-BrdU antibody, and analyzed by ArrayScan. Data are presented as mean ± SD (n = 3). **p < 0. 001.

lethally irradiated CD45-congenic mice together with 1 × 10^6 competitor BM cells (also from CD45 congenic mice). Three months later, donor chimerism in PB was analyzed. The results showed significantly lower chimerism achieved using BM cells derived from the denervated side than that derived from the sham-operated contralateral side (denervated BM cells, 12.4% ± 2.4%: control BM cells, 53.5% ± 6.2%) (Figure 6A), supporting our observation that the frequency of HSCs was reduced by the effects of denervation. We also performed competitive repopulation assays using $CD34^-KSL$ cells purified from denervated BM in comparison with those from control BM and observed no significant difference between them (Figure 6B). These results support the interpretation that the quantity but not the quality of HSCs is responsible for decreased reconstitution activity in denervated BM. To examine the possibility that HSC numbers were reduced in BM because of their mobilization, we examined PB and spleen for the presence of $CD34^-KSL$ HSCs before and after denervation but did not observe any increase of HSCs either in PB or in spleen (Figure 6C; data not shown).

Notably, as was the case with $Tgfbr2^{del/-}Rag2^{-/-}$ HSCs in Figure 1E, the levels of pSmad2/3 were significantly downregulated in HSCs after selective denervation (Figure 6D). To examine cell cycle status, we then isolated HSCs from denervated femora of mice that had been given BrdU for 7 days. The HSCs were stained with FITC-conjugated anti-BrdU antibody and analyzed by ArrayScan. Significantly higher proportions of HSCs isolated from denervated BM were positive for BrdU than of those from control BM (Figure 6E). These data strongly indicate that the glial cell component of the niche is responsible for the maintenance of HSC hibernation in BM by regulating the process by which latent TGF-β is activated.

This concept was supported by the effects of exogenous latent and active TGF-β on HSCs in denervated mice. Beginning 1 week after denervation, either latent or active TGF-β was infused into mice every other day for 1 week, and BrdU-containing water was given throughout the same week. Cell cycle analysis at day 14 after denervation revealed that active TGF-β significantly suppressed active cycling of HSCs in denervated mice, whereas latent TGF-β did not (Figure 6F). These results confirm the cytostatic effect of active TGF-β on HSCs and underline the role of the glial cell component of the niche in converting latent TGF-β into active TGF-β.

DISCUSSION

We have shown in this study that Smad2 and Smad3 are activated in HSCs in BM. $Tgfbr2^{del/-}$ HSCs showed profoundly low levels of Smad2 and Smad3 phosphorylation and were defective

with respect to the long-term repopulating capacity of hematopoiesis. As previously reported (Yamazaki et al., 2006, 2009), TGF-β may tune down cytokine signals by inhibiting cytokine-induced lipid raft clustering. By doing so, TGF-β keeps the PI3K-Akt pathway suppressed and induces cyclins D1, D2, and D3 distancing from the nucleus, whereas it stabilizes FoxO1, 3a, and 4, permitting them to function in the nucleus. TGF-β also activates Smad2 and Smad3 and supposedly regulates transcription of $p57^{Kip2}$ for example, the cyclin-dependent kinase inhibitor gene highly expressed in dormant HSCs (Yamazaki et al., 2006). Regulation of these machineries is reportedly critical to maintenance of the dormant state in HSCs (Oguro and Iwama, 2007; Yilmaz et al., 2006; Zhang et al., 2006; Kozar et al., 2004; Tothova et al., 2007; Miyamoto et al., 2007; Yoshihara et al., 2007). Although the defects in $Tgfbr2^{del/-}$ HSCs were relatively mild compared with those in mice deficient in *Smad4* (Karlsson et al., 2007), which acts at a common level of convergence for all TGF-β superfamily signals, all these in vivo findings define the TGF-β/Smad signal as one of the critical niche signals in the maintenance of HSCs. Correspondingly, a critical role of TGF-β has recently been reported in the maintenance of quiescence and immaturity of melanocyte stem cells (Nishimura et al., 2010). Therefore, the TGF-β signal could have a general impact on the maintenance of stem cell dormancy.

Latent TGF-β, produced by a variety of BM cells, is broadly distributed within BM. However, active TGF-β is exclusively detectable in nonmyelinating Schwann cells that lay in parallel with blood vessels. These glial cells in BM express not only stem cell niche genes, but also *Itgb8*. Upon cell-to-cell contact, integrin-αvβ8 of Schwann cells supposedly binds to LAP and changes the conformation of the latent TGF-β complex. The consequent exposure of the cleavage site for proteolytic degradation by plasmin and metalloproteinases results in production of active TGF-β. Thus, in BM, function of TGF-β appears tightly regulated by an activation process. Active TGF-β triggers the Smad signaling pathway, causing hibernation in HSCs. Given that TGF-βs are prone to degradation, they may act locally at the glial niche without diffusing to distant progenitor cells. That TGF-β should regulate HSCs locally is reasonable if the highly cytostatic activity of TGF-β is to be restricted to dormant HSCs.

Smad2 and Smad3 were activated in most HSCs, whereas only 25% of HSCs were in contact with the glial component of the niche. This finding raises the possibility that HSCs, depending on their activation status, shift among various compartments of the niche. Once Smad2 and Smad3 are activated via the glial component of the niche, HSCs may retain Smads in active form, even after relocation into another compartment, until the HSCs receive cues for cell division. Alternatively, by shifting away from glial cells, Smad signaling is downregulated, and therefore, HSCs may regain the ability to form lipid raft clusters and to be aroused from hibernation to enter the cell cycle. Another possibility is that usage of signaling molecules by different TGF-β superfamily ligands overlaps. Absence of TβRI reportedly does not affect the hematopoietic system (Larsson and Karlsson, 2005). Here, we demonstrated HSC abnormalities in *Tgfbr2*-deficient mice. These observations are in accordance with the fact that *Tgfbr2* is expressed in HSCs, but *Tgfbr1* is not (Utsugisawa et al., 2006; Yamazaki et al., 2009). This adds to the complex roles of ligands, receptors, and Smads in TGF-β signaling in HSCs (Karlsson et al., 2007). A recent study has demonstrated that mice deficient in both Smad1 and Smad5 have no hematopoietic abnormalities (Singbrant et al., 2010). On the other hand, mice deficient in *Smad4* show HSC abnormalities similar to those in *Tgfbr2*-deficient mice (Karlsson et al., 2007). These data suggest that signaling downstream from TβRII but not from bone morphogenetic protein receptors plays a role in the maintenance of HSCs in BM. However, how TGF-β conveys signals into the cell without TβRI remains to be elucidated. TβRI is a member of the ALK family. As far as we and others have been able to determine (Utsugisawa et al., 2006), expression of other members of the ALK family in HSCs is barely detectable. To understand the whole picture of regulation of HSC dormancy by TGF-β superfamily, further characterization is required.

To observe the contribution of the nervous system to hematopoiesis, we performed ischiac nerve denervation (data not shown) as well as selective sympathetic denervation. Surprisingly, in both cases, denervation resulted in significant decreases in the number of BM glial cells and of cells expressing active TGF-β. In parallel we observed a drastic reduction in HSC numbers, with the HSCs present found to be actively cycling. This finding supports the idea that neural regulation plays a role in homeostasis of hematopoiesis. Other studies have also shown that signals from the sympathetic nervous system enhance HSC egression from the BM osteoblastic niche through suppression of Cxcl12 production (Katayama et al., 2006). Circadian noradrenalin secretion by the sympathetic nervous system also regulates *Cxcl12* expression in the BM microenvironment, thereby regulating release of HSCs from their niche (Méndez-Ferrer et al., 2008). Moreover, catecholaminergic pathways can promote human $CD34^+$ cell migration and engraftment by acting directly on HSC/progenitor cells (Spiegel et al., 2007). This sympathetic nerve regulation of HSC maintenance reportedly is mediated indirectly by $Nestin^+$ MSCs expressing β3-adrenergic receptor (Méndez-Ferrer et al., 2010). However, the present work implicates BM glial cells of the autonomic nervous system in direct regulation of HSCs. By regulating the activation process of TGF-β, these glial cells appear to control hibernation of HSCs in BM. How these two components of the BM niche are related in the maintenance of homeostasis of HSCs under the influence of the autonomic nervous system remains an intriguing issue. Identification of glial cells as BM HSC niche components opens up a new area of research that links the neural and hematopoietic systems.

EXPERIMENTAL PROCEDURES

Mice

C57BL/6 (B6-Ly5.2) mice were purchased from SLC (Shizuoka, Japan). C57BL/6 mice congenic for the Ly5 locus (B6-Ly5.1) were bred and maintained at Sankyo Lab Service (Tsukuba, Japan). C57BL/6-Ly5.1/Ly5.2 F_1 mice were used for competitive reconstitution assays. $Tgfbr2^{+/-}Rag2^{-/-}$ mice were obtained by mating $Tgfbr2^{+/-}$ mice (Oshima et al., 1996) with $Rag2^{-/-}$ mice. To generate *Mx-1-Cre;* $Tgfbr2^{flox/-}Rag2^{-/-}$ mice, $Tgfbr2^{flox/+}$ mice (Levéen et al., 2005) were crossed with interferon-inducible *Mx-1-Cre* transgenic mice and $Rag2^{-/-}$ mice. To induce *Cre*, mice received 250 μg of pIpC intraperitoneally three times every other day. *GFAP*-promoter GFP mice have been

described (Suzuki et al., 2003). Mice were bred and maintained at the Animal Research Facility of the Institute of Medical Science, University of Tokyo. Animal care was carried out in accordance with the guidance of the University of Tokyo for animal and recombinant DNA experiments.

Analysis and Purification of Mouse HSCs and CD34$^+$KSL Cells

Mouse CD34$^-$KSL HSCs and CD34$^+$KSL MPPs were purified from BM of 2-month-old mice. The cells were stained with an antibody cocktail consisting of biotinylated anti-Gr-1, -Mac-1, -B220, -CD4, -CD8, and -Ter-119 monoclonal antibodies (lineage-marker cocktail) (PharMingen, San Diego, CA, USA). Lineage-positive cells were depleted with anti-rat MicroBeads (Miltenyi Biotec, Bergisch Gladbach, Germany). The remaining cells were further stained with fluorescein isothiocyanate (FITC)-conjugated anti-CD34, phycoerythrin (PE)-conjugated anti-Sca-1, and allophycocyanin (APC)-conjugated anti-c-Kit antibodies (PharMingen). Biotinylated antibodies were detected with streptavidin-APC-Cy7 (PharMingen). Analysis and cell sorting were performed on a MoFlo using Summit software (Beckman Coulter, Fullerton, CA, USA), and results were analyzed with FlowJo software (Tree Star, Ashland, OR, USA).

Immunofluorescence Staining of BM Sections

Frozen BM sections were prepared and immunostained according to the Kawamoto method (Kawamoto, 2003). BM sections were fixed using dry ice/ethanol or 4% paraformaldehyde (PFA). Immunofluorescence data were obtained and analyzed with a TCS SP2 AOBS confocal microscope (Leica, Microsystems, Tokyo) or a Cellomics ArrayScan VTI HCS Reader (Thermo Scientific, Pittsburgh), a modular high-content screening instrument designed for high-capacity automated fluorescence cell imaging with quantitative analysis. The immunofluorescence-microscopy images of BM sections were automatically obtained, using integrated reader software, from multiple replicates. Markers and antibodies used were: 4,6-diamidino-2-phenylindole (DAPI), a DNA marker; Alexa 405-conjugated goat anti-rabbit IgG, Alexa 488-conjugated goat anti-chicken IgG, and Alexa 647-conjugated goat anti-rabbit IgG (Molecular Probes, Carlsbad, CA, USA); rabbit anti-GFAP (Dako, Glostrup, Denmark); goat anti-LAP (latent TGF-β) and rabbit anti-TGF-β (R&D systems, Minneapolis); rabbit anti-osteocalcin (Lifespan, Seattle); rabbit anti-*Itgb8* and anti-LTPB1 (Santa Cruz Biotechnology, Santa Cruz, CA, USA); rabbit anti-phospho-Smad2/3 (Chemicon, Temecula, CA, USA); chicken anti-neurofilament (Millipore, Billerica, MA, USA); chicken anti-nestin and rabbit anti-S100β (Abcam, Cambridge); rabbit anti-tyrosine hydroxylase (Cell signaling, Charlottesville, VA, USA); and Alexa 488-conjugated rat anti-VE-cadherin, FITC-conjugated rat anti-CD41, FITC-conjugated anti-CD48, FITC-conjugated lineage-marker cocktail, PE-conjugated rat anti-CD150, APC-conjugated rat anti-CD150, and APC-conjugated rat anti-PDGFRα (BioLegend, San Diego, CA, USA).

Immunofluorescence Staining of HSCs

CD34$^-$KSL cells were sorted into a droplet of serum-free culture medium made on glass slides. The sorted cells were incubated at 37°C for the indicated time periods. After fixation with 2% PFA and blocking in 10% goat serum for 1 hr at room temperature, cells were incubated with a primary antibody for 12 hr at 4°C. The cells were then washed and were incubated with a secondary antibody for 30 min at room temperature. Immunofluorescence data were obtained and analyzed with a Cellomics ArrayScan VTI HCS Reader (Thermo Scientific).

Preparation of Primary Schwann Cells

GFAP-positive primary glial cells were prepared from the sciatic nerve of adult C57BL/6 GFAP-GFP mice using forceps under the stereoscopic microscope (Leica, Microsystems, Tokyo).

Competitive Repopulation Assays

Competitive repopulation assays were performed using the Ly5 congenic mouse system. A total of 1 × 10^6 BM cells from *Tgfbr2*$^{del/-}$*Rag2*$^{-/-}$ mice (B6-Ly5.1) and the same number of BM competitor cells from B6-F1 mice of Ly5.1 and 5.2 mice were transplanted into B6-Ly5.2 mice irradiated at a dose of 9.5 Gy. For denervated mice, 1 × 10^6 BM cells or 40 HSCs (B6-Ly5.1) obtained 1 month after denervation and 1 × 10^6 BM competitor cells from B6-F1 mice of Ly5.1 and 5.2 mice were transplanted into B6-Ly5.2 mice irradiated at a dose of 9.5 Gy. After transplantation, PB cells of the recipients were stained with biotinylated anti-Ly5.1 and FITC-conjugated anti-Ly5.2. The cells were further stained with APC-conjugated anti-Mac-1 and -Gr-1 antibodies and with PE-conjugated streptavidin (PharMingen). The cells were analyzed on a FACS Aria (Becton Dickinson, Franklin Lakes, NJ, USA). Percent chimerism was calculated as (percent Ly5.1 cells) × 100/(percent Ly5.1 cells + percent F1 cells).

RT-PCR

Semiquantitative RT-PCR was carried out using cDNA normalized by quantitative PCR with TaqMan rodent GAPDH control reagent (Perkin-Elmer Applied Biosystems, Foster City, CA, USA). The primer sequences were: *Itgb8* sense 5′-CCTGCAGTGAAAACTGGA-3′, antisense 5′-TTT CTC ACG TCG GTA GGT-3′; *Cxcl12* sense 5′-GCA TCA GTG ACG GTA AAC CAG-3′, antisense 5′-GGG TCA ATG CAC ACT TGT CTG-3′; *kitl* sense 5′-GAA TCT CCG AAG AGG CCA GAA ACT AGA TCC TTT-3′, antisense 5′-CGT CCA CAA TTA CAC CTC TTG AAA TTC TCT CTC-3′; *Angpt1* sense 5′-CAT TCT TCG CTG CCA TTC TG-3′; antisense 5′-GCA CAT TGC CCA TGT TGA ATC-3′; and *Tpo* sense 5′-CCT CTT CTT GAG CTT GCA AC-3′; antisense 5′-AGC CAT GAG TTC CAT TCA C-3′. Cycling parameters were: denaturation at 95°C for 15 s, annealing at 58°C for 15 s, and extension at 72°C for 30 s. Amplification proceeded for 38 or 40 cycles. PCR products were separated on agarose gels and were visualized by ethidium bromide staining.

Denervation of BM

The lumbar sympathetic trunk was cut unilaterally at the level of L2, L3, and L4 to denervate sympathetic nerves to the biceps femoris muscle and the BM. After the wounds were sutured, the animals were returned to their cages for 3–30 days before sacrifice and study. This surgical procedure spares motor and sensory nerves, leaving the animal's motion intact (Noguchi et al., 1999).

Cell Cycle Analysis

To investigate the turnover rate of CD34$^-$KSL cells, BrdU (Sigma-Aldrich) was administered continuously to mice via drinking water (0.5 mg/ml). After 1 week, CD34$^-$KSL cells were isolated and stained with FITC-conjugated anti-BrdU antibody (Molecular Probes). The cells then were analyzed by ArrayScan.

Administration of TGF-β to Denervated Mice

Beginning on the seventh day after denervation, either latent TGF-β (recombinant human LAP [TGF-β1]; R&D Systems) or active TGF-β (recombinant human TGF-β1; R&D Systems) was infused intraperitoneally into mice every other day at a dose of 40 μg/kg.

SUPPLEMENTAL INFORMATION

Supplemental Information includes six figures and one movie and can be found with this article online at doi:10.1016/j.cell.2011.09.053.

ACKNOWLEDGMENTS

We thank Y. Yamazaki, Y. Ishii, and Y. Koyama for excellent technical support, Drs. T. Saito and S. Uchida for valuable discussions, and Dr. N. Watanabe, Dr. R. Yamamoto, Dr. T. Kobayashi, N. Suzuki, F. Lin, and Dr. A. Knisely for critical reading of the manuscript. This work was supported by grants from JST, the Ministry of Education, Culture, Sport, Science, and Technology, Japan. H.N. is a founder and shareholder of ReproCELL, Inc.

Received: August 30, 2010
Revised: April 12, 2011
Accepted: September 6, 2011
Published: November 23, 2011

REFERENCES

Annes, J.P., Munger, J.S., and Rifkin, D.B. (2003). Making sense of latent TGFbeta activation. J. Cell Sci. *116*, 217–224.

Annes, J.P., Chen, Y., Munger, J.S., and Rifkin, D.B. (2004). Integrin alphaV-beta6-mediated activation of latent TGF-beta requires the latent TGF-beta binding protein-1. J. Cell Biol. *165*, 723–734.

Arai, F., Hirao, A., Ohmura, M., Sato, H., Matsuoka, S., Takubo, K., Ito, K., Koh, G.Y., and Suda, T. (2004). Tie2/angiopoietin-1 signaling regulates hematopoietic stem cell quiescence in the bone marrow niche. Cell *118*, 149–161.

Bradford, G.B., Williams, B., Rossi, R., and Bertoncello, I. (1997). Quiescence, cycling, and turnover in the primitive hematopoietic stem cell compartment. Exp. Hematol. *25*, 445–453.

Calvi, L.M., Adams, G.B., Weibrecht, K.W., Weber, J.M., Olson, D.P., Knight, M.C., Martin, R.P., Schipani, E., Divieti, P., Bringhurst, F.R., et al. (2003). Osteoblastic cells regulate the haematopoietic stem cell niche. Nature *425*, 841–846.

Calvo, W., and Forteza-Vila, J. (1970). Schwann cells of the bone marrow. Blood *36*, 180–188.

Cambier, S., Gline, S., Mu, D., Collins, R., Araya, J., Dolganov, G., Einheber, S., Boudreau, N., and Nishimura, S.L. (2005). Integrin alpha(v)beta8-mediated activation of transforming growth factor-beta by perivascular astrocytes: an angiogenic control switch. Am. J. Pathol. *166*, 1883–1894.

Chernousov, M.A., and Carey, D.J. (2003). alphaVbeta8 integrin is a Schwann cell receptor for fibrin. Exp. Cell Res. *291*, 514–524.

Cheshier, S.H., Morrison, S.J., Liao, X., and Weissman, I.L. (1999). In vivo proliferation and cell cycle kinetics of long-term self-renewing hematopoietic stem cells. Proc. Natl. Acad. Sci. USA *96*, 3120–3125.

Coulombe, P.A., and Wong, P. (2004). Cytoplasmic intermediate filaments revealed as dynamic and multipurpose scaffolds. Nat. Cell Biol. *6*, 699–706.

D'Antonio, M., Droggiti, A., Feltri, M.L., Roes, J., Wrabetz, L., Mirsky, R., and Jessen, K.R. (2006). TGFbeta type II receptor signaling controls Schwann cell death and proliferation in developing nerves. J. Neurosci. *26*, 8417–8427.

Fernando, F.S., Conforti, L., Tosi, S., Smith, A.D., and Coleman, M.P. (2002). Human homologue of a gene mutated in the slow Wallerian degeneration (C57BL/Wld(s)) mouse. Gene *284*, 23–29.

Foudi, A., Hochedlinger, K., Van Buren, D., Schindler, J.W., Jaenisch, R., Carey, V., and Hock, H. (2009). Analysis of histone 2B-GFP retention reveals slowly cycling hematopoietic stem cells. Nat. Biotechnol. *27*, 84–90.

Grinspan, J.B., Marchionni, M.A., Reeves, M., Coulaloglou, M., and Scherer, S.S. (1996). Axonal interactions regulate Schwann cell apoptosis in developing peripheral nerve: neuregulin receptors and the role of neuregulins. J. Neurosci. *16*, 6107–6118.

Guérette, D., Khan, P.A., Savard, P.E., and Vincent, M. (2007). Molecular evolution of type VI intermediate filament proteins. BMC Evol. Biol. *7*, 164.

Jessen, K.R., and Mirsky, R. (2005). The origin and development of glial cells in peripheral nerves. Nat. Rev. Neurosci. *6*, 671–682.

Karlsson, G., Blank, U., Moody, J.L., Ehinger, M., Singbrant, S., Deng, C.X., and Karlsson, S. (2007). Smad4 is critical for self-renewal of hematopoietic stem cells. J. Exp. Med. *204*, 467–474.

Katayama, Y., Battista, M., Kao, W.M., Hidalgo, A., Peired, A.J., Thomas, S.A., and Frenette, P.S. (2006). Signals from the sympathetic nervous system regulate hematopoietic stem cell egress from bone marrow. Cell *124*, 407–421.

Kawamoto, T. (2003). Use of a new adhesive film for the preparation of multi-purpose fresh-frozen sections from hard tissues, whole-animals, insects and plants. Arch. Histol. Cytol. *66*, 123–143.

Kiel, M.J., and Morrison, S.J. (2008). Uncertainty in the niches that maintain haematopoietic stem cells. Nat. Rev. Immunol. *8*, 290–301.

Kiel, M.J., Yilmaz, O.H., Iwashita, T., Yilmaz, O.H., Terhorst, C., and Morrison, S.J. (2005). SLAM family receptors distinguish hematopoietic stem and progenitor cells and reveal endothelial niches for stem cells. Cell *121*, 1109–1121.

Kozar, K., Ciemerych, M.A., Rebel, V.I., Shigematsu, H., Zagozdzon, A., Sicinska, E., Geng, Y., Yu, Q., Bhattacharya, S., Bronson, R.T., et al. (2004). Mouse development and cell proliferation in the absence of D-cyclins. Cell *118*, 477–491.

Larsson, J., and Karlsson, S. (2005). The role of Smad signaling in hematopoiesis. Oncogene *24*, 5676–5692.

Levéen, P., Carlsén, M., Makowska, A., Oddsson, S., Larsson, J., Goumans, M.J., Cilio, C.M., and Karlsson, S. (2005). TGF-beta type II receptor-deficient thymocytes develop normally but demonstrate increased CD8+ proliferation in vivo. Blood *106*, 4234–4240.

Lyons, R.M., Gentry, L.E., Purchio, A.F., and Moses, H.L. (1990). Mechanism of activation of latent recombinant transforming growth factor beta 1 by plasmin. J. Cell Biol. *110*, 1361–1367.

Méndez-Ferrer, S., Lucas, D., Battista, M., and Frenette, P.S. (2008). Haematopoietic stem cell release is regulated by circadian oscillations. Nature *452*, 442–447.

Méndez-Ferrer, S., Michurina, T.V., Ferraro, F., Mazloom, A.R., Macarthur, B.D., Lira, S.A., Scadden, D.T., Ma'ayan, A., Enikolopov, G.N., and Frenette, P.S. (2010). Mesenchymal and haematopoietic stem cells form a unique bone marrow niche. Nature *466*, 829–834.

Miyamoto, K., Araki, K.Y., Naka, K., Arai, F., Takubo, K., Yamazaki, S., Matsuoka, S., Miyamoto, T., Ito, K., Ohmura, M., et al. (2007). Foxo3a is essential for maintenance of the hematopoietic stem cell pool. Cell Stem Cell *1*, 101–112.

Morikawa, S., Mabuchi, Y., Niibe, K., Suzuki, S., Nagoshi, N., Sunabori, T., Shimmura, S., Nagai, Y., Nakagawa, T., Okano, H., and Matsuzaki, Y. (2009). Development of mesenchymal stem cells partially originate from the neural crest. Biochem. Biophys. Res. Commun. *379*, 1114–1119.

Morrison, S.J., Hemmati, H.D., Wandycz, A.M., and Weissman, I.L. (1995). The purification and characterization of fetal liver hematopoietic stem cells. Proc. Natl. Acad. Sci. USA *92*, 10302–10306.

Mu, D., Cambier, S., Fjellbirkeland, L., Baron, J.L., Munger, J.S., Kawakatsu, H., Sheppard, D., Broaddus, V.C., and Nishimura, S.L. (2002). The integrin alpha(v)beta8 mediates epithelial homeostasis through MT1-MMP-dependent activation of TGF-beta1. J. Cell Biol. *157*, 493–507.

Munger, J.S., Huang, X., Kawakatsu, H., Griffiths, M.J., Dalton, S.L., Wu, J., Pittet, J.F., Kaminski, N., Garat, C., Matthay, M.A., et al. (1999). The integrin alpha v beta 6 binds and activates latent TGF beta 1: a mechanism for regulating pulmonary inflammation and fibrosis. Cell *96*, 319–328.

Murinson, B.B., and Griffin, J.W. (2004). C-fiber structure varies with location in peripheral nerve. J. Neuropathol. Exp. Neurol. *63*, 246–254.

Nishimura, E.K., Suzuki, M., Igras, V., Du, J., Lonning, S., Miyachi, Y., Roes, J., Beermann, F., and Fisher, D.E. (2010). Key roles for transforming growth factor beta in melanocyte stem cell maintenance. Cell Stem Cell *6*, 130–140.

Noguchi, E., Ohsawa, H., Kobayashi, S., Shimura, M., Uchida, S., and Sato, Y. (1999). The effect of electro-acupuncture stimulation on the muscle blood flow of the hindlimb in anesthetized rats. J. Auton. Nerv. Syst. *75*, 78–86.

Oguro, H., and Iwama, A. (2007). Life and death in hematopoietic stem cells. Curr. Opin. Immunol. *19*, 503–509.

Omatsu, Y., Sugiyama, T., Kohara, H., Kondoh, G., Fujii, N., Kohno, K., and Nagasawa, T. (2010). The essential functions of adipo-osteogenic progenitors as the hematopoietic stem cell and progenitor cells niche. Immunity *33*, 387–399.

Oshima, M., Oshima, H., and Taketo, M.M. (1996). TGF-beta receptor type II deficiency results in defects of yolk sac hematopoiesis and vasculogenesis. Dev. Biol. *179*, 297–302.

Rosendahl, A., Speletas, M., Leandersson, K., Ivars, F., and Sideras, P. (2003). Transforming growth factor-beta- and Activin-Smad signaling pathways are activated at distinct maturation stages of the thymopoeisis. Int. Immunol. *15*, 1401–1414.

Schmierer, B., and Hill, C.S. (2007). TGFbeta-SMAD signal transduction: molecular specificity and functional flexibility. Nat. Rev. Mol. Cell Biol. *8*, 970–982.

Singbrant, S., Karlsson, G., Ehinger, M., Olsson, K., Jaako, P., Miharada, K., Stadtfeld, M., Graf, T., and Karlsson, S. (2010). Canonical BMP signaling is dispensable for hematopoietic stem cell function in both adult and fetal liver hematopoiesis, but essential to preserve colon architecture. Blood *115*, 4689–4698.

Spiegel, A., Shivtiel, S., Kalinkovich, A., Ludin, A., Netzer, N., Goichberg, P., Azaria, Y., Resnick, I., Hardan, I., Ben-Hur, H., et al. (2007). Catecholaminergic neurotransmitters regulate migration and repopulation of immature human CD34+ cells through Wnt signaling. Nat. Immunol. *8*, 1123–1131.

Sudo, K., Ema, H., Morita, Y., and Nakauchi, H. (2000). Age-associated characteristics of murine hematopoietic stem cells. J. Exp. Med. *192*, 1273–1280.

Sugiyama, T., Kohara, H., Noda, M., and Nagasawa, T. (2006). Maintenance of the hematopoietic stem cell pool by CXCL12-CXCR4 chemokine signaling in bone marrow stromal cell niche. Immunity *25*, 977–988.

Sulaiman, O.A., Midha, R., Munro, C.A., Matsuyama, T., Al-Majed, A., and Gordon, T. (2002). Chronic Schwann cell denervation and the presence of a sensory nerve reduce motor axonal regeneration. Exp. Neurol. *176*, 342–354.

Suzuki, R., Arata, S., Nakajo, S., Ikenaka, K., Kikuyama, S., and Shioda, S. (2003). Expression of the receptor for pituitary adenylate cyclase-activating polypeptide (PAC1-R) in reactive astrocytes. Brain Res. Mol. Brain Res. *115*, 10–20.

Tothova, Z., Kollipara, R., Huntly, B.J., Lee, B.H., Castrillon, D.H., Cullen, D.E., McDowell, E.P., Lazo-Kallanian, S., Williams, I.R., Sears, C., et al. (2007). FoxOs are critical mediators of hematopoietic stem cell resistance to physiologic oxidative stress. Cell *128*, 325–339.

Utsugisawa, T., Moody, J.L., Aspling, M., Nilsson, E., Carlsson, L., and Karlsson, S. (2006). A road map toward defining the role of Smad signaling in hematopoietic stem cells. Stem Cells *24*, 1128–1136.

Waite, K.A., and Eng, C. (2003). From developmental disorder to heritable cancer: it's all in the BMP/TGF-beta family. Nat. Rev. Genet. *4*, 763–773.

Yamazaki, S., Iwama, A., Takayanagi, S., Morita, Y., Eto, K., Ema, H., and Nakauchi, H. (2006). Cytokine signals modulated via lipid rafts mimic niche signals and induce hibernation in hematopoietic stem cells. EMBO J. *25*, 3515–3523.

Yamazaki, S., Iwama, A., Takayanagi, S., Eto, K., Ema, H., and Nakauchi, H. (2009). TGF-beta as a candidate bone marrow niche signal to induce hematopoietic stem cell hibernation. Blood *113*, 1250–1256.

Yilmaz, O.H., Valdez, R., Theisen, B.K., Guo, W., Ferguson, D.O., Wu, H., and Morrison, S.J. (2006). Pten dependence distinguishes haematopoietic stem cells from leukaemia-initiating cells. Nature *441*, 475–482.

Yoshihara, H., Arai, F., Hosokawa, K., Hagiwara, T., Takubo, K., Nakamura, Y., Gomei, Y., Iwasaki, H., Matsuoka, S., Miyamoto, K., et al. (2007). Thrombopoietin/MPL signaling regulates hematopoietic stem cell quiescence and interaction with the osteoblastic niche. Cell Stem Cell *1*, 685–697.

Zhang, J., Niu, C., Ye, L., Huang, H., He, X., Tong, W.G., Ross, J., Haug, J., Johnson, T., Feng, J.Q., et al. (2003). Identification of the hematopoietic stem cell niche and control of the niche size. Nature *425*, 836–841.

Zhang, J., Grindley, J.C., Yin, T., Jayasinghe, S., He, X.C., Ross, J.T., Haug, J.S., Rupp, D., Porter-Westpfahl, K.S., Wiedemann, L.M., et al. (2006). PTEN maintains haematopoietic stem cells and acts in lineage choice and leukaemia prevention. Nature *441*, 518–522.

OPEN ACCESS Freely available online

PLoS one

Generation of Germline-Competent Rat Induced Pluripotent Stem Cells

Sanae Hamanaka[1,2], Tomoyuki Yamaguchi[1,2]*, Toshihiro Kobayashi[1,2], Megumi Kato-Itoh[2], Satoshi Yamazaki[2], Hideyuki Sato[2], Ayumi Umino[2], Yukiko Wakiyama[2], Mami Arai[2], Makoto Sanbo[3], Masumi Hirabayashi[3,4], Hiromitsu Nakauchi[1,2]*

1 Japan Science Technology Agency, Exploratory Research for Advanced Technology (ERATO), Nakauchi Stem Cell and Organ Regeneration Project, Tokyo, Japan, **2** Division of Stem Cell Therapy, Center for Stem Cell Biology and Regenerative Medicine, Institute of Medical Science, University of Tokyo, Tokyo, Japan, **3** Center for Genetic Analysis of Behavior, National Institute for Physiological Sciences, Okazaki, Japan, **4** School of Life Science, The Graduate University for Advanced Studies, Okazaki, Japan

Abstract

Background: Recent progress in rat pluripotent stem cell technology has been remarkable. Particularly salient is the demonstration that embryonic stem cells (ESCs) in the rat (rESCs) can contribute to germline transmission, permitting generation of gene-modified rats as is now done using mouse ESCs (mESCs) or mouse induced pluripotent stem cells (iPSCs; miPSCs). However, determinations of whether rat iPSCs (riPSCs) can contribute to germ cells are not published. Here we report the germline competency of riPSCs.

Methodology/Principal Findings: We generated riPSCs by transducing three mouse reprogramming factors (Oct3/4, Klf4, and Sox2) into rat somatic cells, followed by culture in the presence of exogenous rat leukemia inhibitory factor (rLIF) and small molecules that specifically inhibit GSK3, MEK, and FGF receptor tyrosine kinases. We found that, like rESCs, our riPSCs can contribute to germline transmission. Furthermore we found, by immunostaining of testis from mouse-rat interspecific chimeras with antibody against mouse vasa homolog, that riPSCs can contribute to embryonic development with chimera formation in mice (rat-mouse interspecific chimeras) and to interspecific germlines.

Conclusions/Significance: Our data clearly demonstrate that using only three reprogramming factors (Oct3/4, Klf4, and Sox2) rat somatic cells can be reprogrammed into a ground state. Our generated riPSCs exhibited germline transmission in either rat-rat intraspecific or mouse-rat interspecific chimeras.

Citation: Hamanaka S, Yamaguchi T, Kobayashi T, Kato-Itoh M, Yamazaki S, et al. (2011) Generation of Germline-Competent Rat Induced Pluripotent Stem Cells. PLoS ONE 6(7): e22008. doi:10.1371/journal.pone.0022008

Editor: Domingos Henrique, Instituto de Medicina Molecular, Portugal

Received April 13, 2011; **Accepted** June 10, 2011; **Published** July 15, 2011

Funding: This work was supported by grants from the Japan Science and Technology Agency, the Ministry of Education, Culture, Sport, Science, and Technology, Japan, and in part by the Cooperative Study Program of National Institute for Physiological Sciences, Japan. The funders had no role in study design, data collection and analysis, decision to publish, or preparation of the manuscript.

Competing Interests: The authors have declared that no competing interests exist.

* E-mail: tomoyama@ims.u-tokyo.ac.jp (TY); nakauchi@ims.u-tokyo.ac.jp (HN)

Introduction

Mouse embryonic stem cells (ESCs), first established in 1981, were originally generated from the inner cell mass of mouse blastocysts. Because they are pluripotent, have potentially unlimited capacity for self-renewal, and can contribute to transmitted germlines (exhibit germline competency), mouse ESCs (mESCs) have constituted powerful tools when generating genetically modified mice to understand gene functions and to create mouse models for human diseases [1]. In 2006, Yamanaka et al. reported the generation of pluripotent stem cells from mouse somatic cells by the enforced expression of four transcription factors (Oct3/4, Sox2, c-Myc, and Klf4) selected from genes known to be expressed in ESCs. They referred to these cells as induced pluripotent stem cells (iPSCs). Like mESCs, which they resemble, mouse iPSCs (miPSCs) express alkaline phosphatase (ALP), can generate chimeric mice, and can take part in germline transmission [2] [3]. The discovery of iPSCs, a great step forward in stem-cell research, holds out the promise of development of novel therapeutic strategies by generating iPSCs from patients. Since 2006, besides mESCs and miPSCs, pluripotent stem cells from several mammalian species have been established, including rat [4] [5] [6] [7], rabbit [8] [9], pig [10] [11], monkey [12] [13] [14], and human [15] [16] [17]. Although such iPSCs express a panel of pluripotency markers like SSEA-1, 3, 4, ALP, and Oct3/4, only mESCs and miPSCs can generate chimeras. However, remarkable progress has been made recently, and rat pluripotent stem cell technology now is capable of generating chimeric rats. In 2008, Ying et al. reported establishment of rat ESCs (rESCs) with use of two or three kinds of kinase inhibitors, including glycogen synthase kinase 3 (GSK3) inhibitor, mitogen-activated protein kinase kinase (MEK) inhibitor, and fibroblast growth factor (FGF) receptor tyrosine kinase inhibitor in the culture medium. These inhibitors have been thought to maintain a ground state of pluripotency in mESCs [18] and can support efficient derivation and maintenance of rESCs, permitting generation of chimeric rats, with germline transmission [19] [20].

Shortly after establishment of rESCs, rat iPSCs (riPSCs) also were successfully established. As riPSCs can differentiate into all three germ layers *in vitro* and *in vivo* [21] [22], and can contribute to generating chimeric rat [16]. However, germline competency of riPSCs has not been reported to date.

The rat has been used as a model for studies of physiology, pharmacology, toxicology, nutrition, behavior, immunology, and neoplasia. Its size, its ease of manipulation, and the availability of many kinds of spontaneous models for diseases such as hypertension and diabetes have made the rat the preferred choice for most of these fields, while the mouse has become the leading mammal for experimental genetics. To extend experimental genetics into the rat could be of great value: Generation of iPSCs from disease-model rats could help clarify the pathogenesis of various disorders, particularly if germline-competent iPSCs are necessary to demonstrate curative effects, as when the mutated gene that is responsible for disease can be corrected in riPSCs by homologous recombination and the curative effect can be observed in F1 rats derived from gene-corrected riPSCs.

Here we report for the first time that adding two or three kinds of kinase inhibitor and rLIF to culture medium can generate germline-competent riPSCs. Moreover, we generated reprogrammable rats from riPSCs that were created by infection of three reprogramming factors (*Oct3/4*, *Klf4*, and *Sox2*) via an inducible lentiviral vector.

Results

Generation of riPSCs from rat embryonic fibroblasts

To generate germline-competent riPSCs, we initially infected Wistar (WI) or Dark Agouti (DA) rat embryonic fibroblasts (REFs) from embryonic day 14.5 or 15.5 (E14.5 or E15.5) with a lentiviral vector carrying three mouse reprogramming factors (*Oct3/4*, *Klf4*, and *Sox2*) controlled by a tetracycline-responsive regulatory element and with *Ubc*-promoter - driven reverse tet transactivator (rtTA) and EGFP (Fig. 1A). We added doxycycline (Dox) to the culture medium on the day of infection (day 0), with rat LIF (rLIF) added to medium on day 1.

Infected REFs were seeded onto mitomycin-C treated mouse embryonic fibroblasts (MEFs) and the medium was changed to serum-free medium (N2B27/F12) containing Dox and rLIF on day 3. On day 7 MEK inhibitor (PD0325901) and GSK3 inhibitor (CHIR99025; 2i) or 2i and FGF receptor inhibitor (SU5409; 3i) were added to the medium (Fig. 1B).

Morphologically ES-like colonies appeared from day 10. They expressed *EGFP* and were of typical dome shape (Fig. 1C). Independent colonies were selected and each colony was expanded in N2B27/F12 medium containing rLIF, 2i, or 3i and with or without Dox. These riPSCs could be sustained for over 25 passages. All ES-like colonies stained for ALP, indicating that generated riPSCs were pluripotent (Fig. 1D). Finally we isolated several riPS clones from both WI and DA fibroblast and chose six clones from WI (T1-3 (referred as riPS#3 in our previous report [23]), T1-4, T1-15, T3-2, T3-3 and T3-11) and two clones from DA (T4-27 and T4-30) for further analysis.

Pluripotency of iPS cells

To evaluate the pluripotency of riPSCs further, we immunostained riPSCs with antibodies against *Nanog* and *Oct3/4* (markers of pluripotency) [16] [24] [25]. RiPSCs expressed both *Nanog* and *Oct3/4* (Fig. 2A). We also examined by RT-PCR the expression of pluripotency marker genes, including *Oct3/4*, *Klf4*, *Fgf4*, *Eras*, *Rex1*, and *Tdgf2*. To detect transgene expression, we designed the primers to amplify sequence between *T2A* and *Sox2*. As shown in Fig. 2B, transgene expression was detected only under with Dox addition, indicating that expression via the lentiviral vector was tightly controlled by a tetracycline-responsive element. We also found that pluripotent marker genes were expressed at levels comparable to those in rESCs; the presence of Dox made no difference (Fig. 2B). The distal enhancer of *Oct3/4* expression reportedly is un-methylated in ESCs (a feature of pluripotency) [26]. To analyze DNA methylation status in riPSCs, we conducted bisulfite-sequencing analysis of genomic regions within the distal enhancer of *Oct3/4* in riPSCs and rESCs. In rESCs and riPSCs the distal enhancer of *Oct3/4* was largely unmethylated, consistent with results from immunostaining and RT-PCR (Fig. 2C). By contrast, in REFs, where *Oct3/4* expression was silenced, the *Oct3/4* enhancer was highly methylated (Fig. 2C).

Next we examined the capacity of riPSCs for *in vivo* differentiation. We injected $0.5–1\times10^6$ riPSCs into testis of non-obese diabetic/severe combined immune deficient mice and assessed teratoma formation, with microscopy of hematoxylin/eosin (HE) - stained sections, 4 to 10 weeks after injection. Tumors reached 15 mm or more in diameter and included elements derived from three germ layers (muscle, cartilage, neural tissues, epidermis, gut-like tissues). These results indicate that our riPSCs had been reprogrammed into a pluripotent state and, like ESCs, possessed the capacity for differentiation into three germ layers (Fig. 2D).

Generation of chimeric rats

Before attempting to generate chimeric rats, we evaluated riPSC karyotypes; they were normal (42XY; Fig. 3A). However, trisomy of chromosome 9 was encountered in clones T1-3, T1-4 and T1-15 (rate: 2/50, 6/50 and 3/50 respectively) cultured with 3i (Figure S1), as observed [20]. As no chromosome abnormality was found in clones T3-2, T3-3 and T3-11 derived from cells cultured with 2i, we continued to culture riPSCs with 2i thereafter. Next we examined the effect of Dox in culture medium on generation of chimeras. WI riPSCs cultured with Dox or without Dox were injected into (WI×WI) rat blastocysts. EGFP expression was assessed by fluorescence microscopy of E15.5 embryos. Using riPSCs cultured with Dox until blastocyst injection, chimeric rat embryos were generated at a ratio of 66%; without Dox, the rate was 100%. Because half life of Dox is 24 hrs, transgene expression continues in embryo after blastocyst injection. This continuous expression of transgene in embryo might influence the chimera contribution. Therefore, for efficient generation of chimeric rat, we cultured riPSCs without Dox thereafter (Fig. 3B, Table 1).

Next we injected riPSCs from clone T1-3 into (DA×WI) F1 blastocysts to permit identification of chimeras by coat color. Using foster mothers and 43 blastocysts into which riPSCs were injected, we obtained four pups of which two were chimeras (Table 1).

Because rat (DA×WI) F1 blastocysts might have potentially low reproduction ability, we then tried to generate chimeras by using rat (WI×WI) blastocysts, detecting chimerism by evaluating expression of EGFP. We obtained 11 chimeras in 18 liveborn pups using clone T1-3 and 7 chimeras in 13 liveborn pups using clone T3-11. We also injected T4-27 and T4-30 into rat (WI×WI) blastcysts and obtained 2 chimeras in 6 liveborn pups and 15 chimeras in 26 liveborn pups respectively (Fig. 3C, Table 1).

These results indicate that riPSCs generated in medium containing 2i can contribute to generating chimeric rats.

Germline transmission of riPSCs

To address whether these riPSCs could contribute to germline transmission, generated male chimeric rats were mated with wild-type female WI rats.

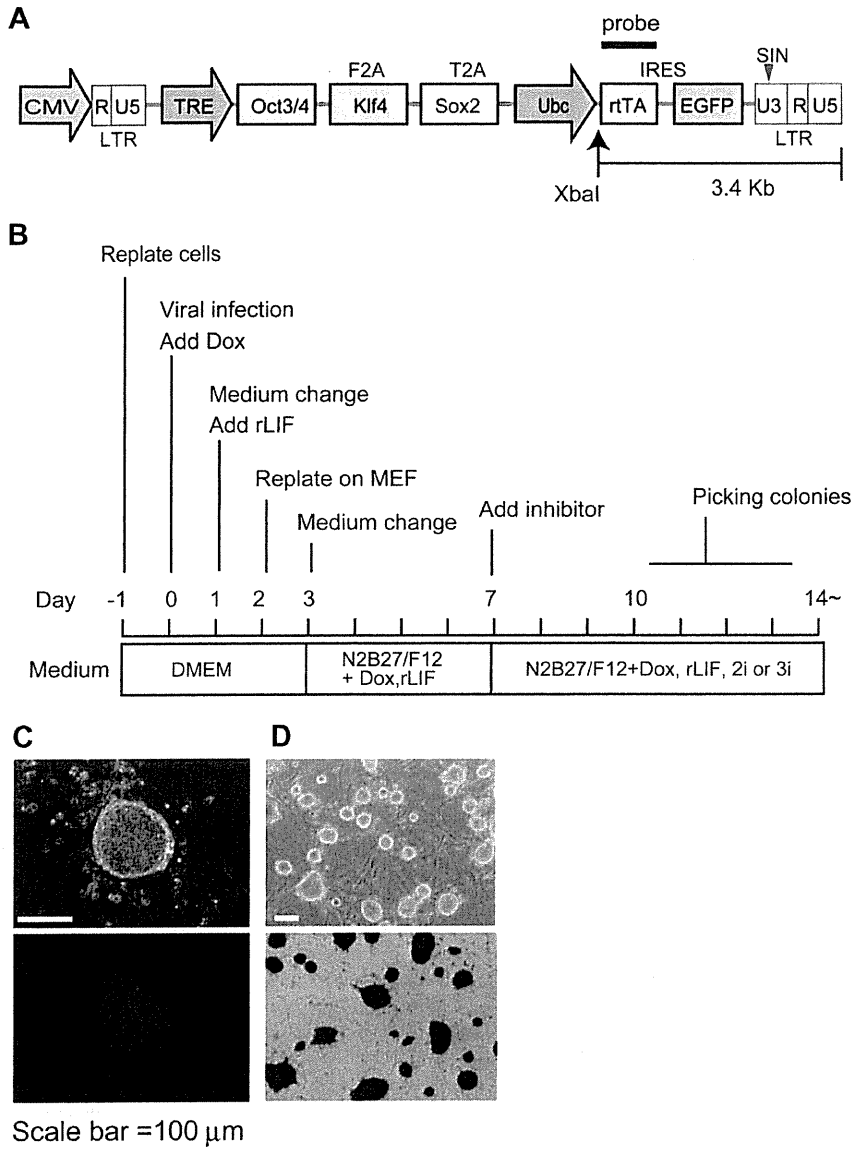

Figure 1. Generation of rat iPS cells from rat embryonic fibroblasts. (A) Schema of inducible lentivirus vector. XbaI enzyme restriction site exists between Ubiquitin-C (*Ubc*) promoter and reverse tet transactivator (rtTA) element. (B) Schematic time schedule of riPSCs generation. (C)–(D) Morphology of generated riPSCs (passage P0); bright field and fluorescent field (C). ALP staining after clonal passage (D).
doi:10.1371/journal.pone.0022008.g001

We obtained three embryos (E15.5) and eight pups that expressed EGFP from three chimeric rats derived from riPSC clones T1-3 or T3-11 (Fig. 4A, Table 1, Table S1). FACS analysis revealed that REFs established from F1 rats also expressed EGFP (Fig. 4B) and, as shown in Fig. 4C, proviral DNA was detected by genomic PCR. For further confirmation of the germline transmission of riPSCs, we attempted to regenerate riPSCs from fibroblasts of F1 rats. Because the clone T1-3 riPSCs from which F1 rats were generated were established using a Dox-inducible lentiviral vector, exposure to Dox should allow riPSCs to regenerate from F1 rat somatic cells. REFs from F1 rats seeded on MEFs and cultured in medium containing Dox. ESC-like colonies began to appear from day 10 and by day 16 and 2,000 REFs had given rise to 16.6 ES-like colonies (triplicate assay; Fig.4E). The frequency of regeneration, calculated as the number of colonies/2000×100 was 1% on day 16 and 4.7% on day 20.

Chimeras derived from riPSC clones T4-27 and DA T4-30 had no offspring that expressed EGFP or had black eyes (Because eye color of DA is black and of WI is red, we can identify F1 rat by black eye color).

However, we found that the seminiferous tubules of these DA chimeras expressed EGFP (Figure S2A). Moreover, immunostaining revealed that germ cells in testis from chimeric rats which were derived from riPSC clone T4-30, contained mouse vasa homolog (MVH) and EGFP double positive cells, indicating that clone T4-30 riPSCs can contribute to germ line transmission (Figure S2B). On the other hand, we could not detect MVH and EGFP double

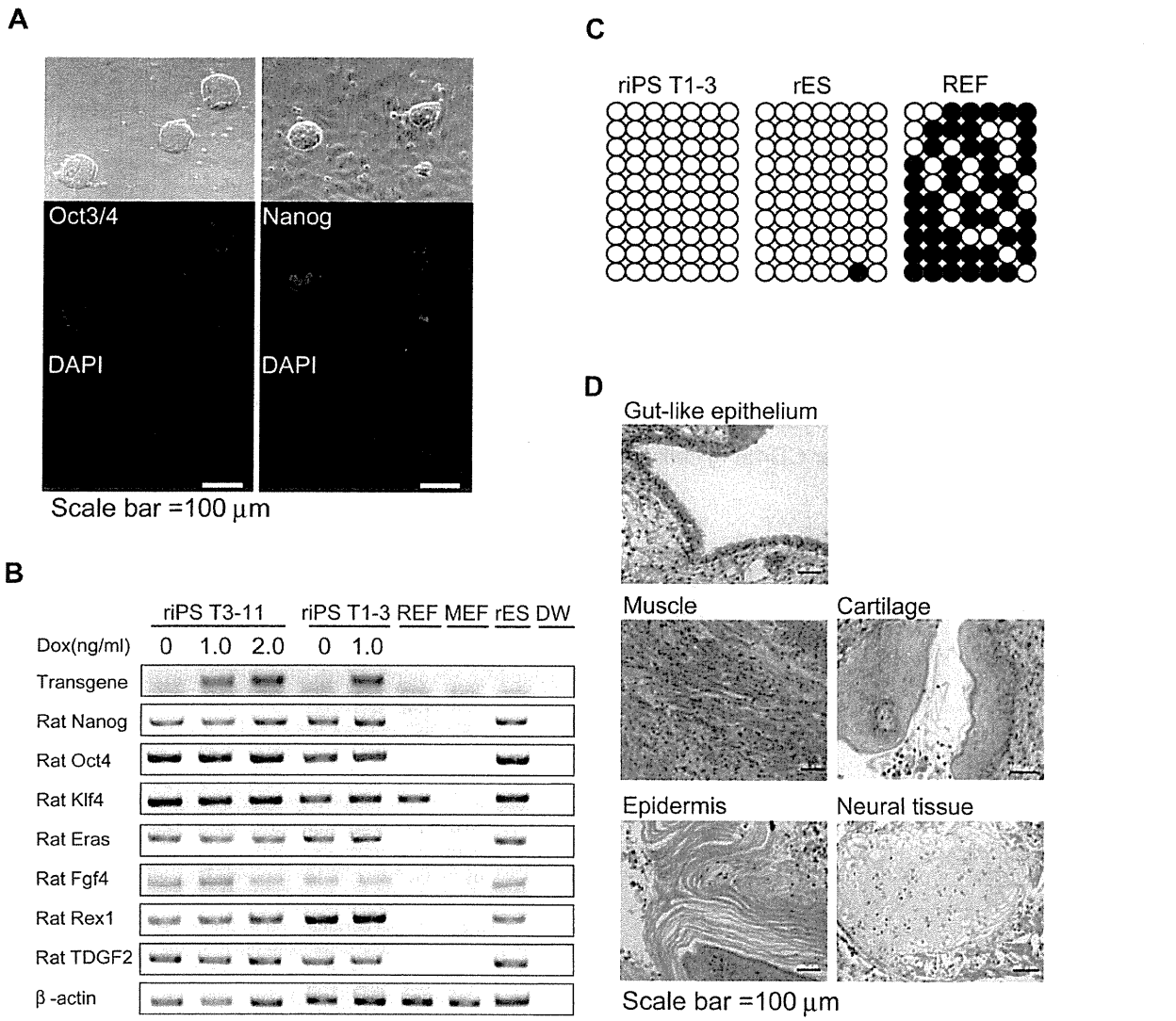

Figure 2. Characterization of rat iPS cells. (A) Immunofluorescence staining for Oct3/4 and Nanog in rat iPS cells (riPSCs). (B) RT-PCR analysis of transgene *T2A-Sox2* and endogenous ES marker genes with or without doxycycline culture. RiPSC clones (riPSCs WI T3-11 and T1-3) express ESC markers. Rat and mouse embryonic fibroblast cells (REFs or MEFs) were used as negative controls. β-actin was used as a loading control. (C) Bisulfite genomic sequencing of the distal enhancer region of *Oct3/4*. Open and closed circles indicate unmethylated and methylated CpGs, respectively. (D) Hematoxylin/eosin staining of teratoma derived from rat iPS cells. Teratoma is composed of various types of tissues: Gut-like epithelium (endoderm), muscle and cartilage (mesoderm), epidermis, and neural tissue (ectoderm).
doi:10.1371/journal.pone.0022008.g002

positive cells in testis from chimeras derived from clone T4-27 riPSCs (data not shown).

To confirm provirus copy number, genomic DNA from riPSCs and from F1 REFs were analyzed by Southern blot (Fig. 4D). Four riPSC lines (lanes 1–4) showed different integration patterns containing one to three transgenes. Progeny derived from clone T1-3 riPSCs (lanes 5–7) carried provirus copies inherited from their riPSCs of origin. Either two or three provirus copies were integrated into the genomes of F1 rats (Table S1).

Tumorigenesis has been observed in chimeric mice (and their offspring) derived from iPSCs generated by transduction of four reprogramming factors (*c-Myc*, *Oct4*, *Sox2*, and *Klf4*), and has been ascribed to reactivation of c-Myc [3]. In our study, however, no tumors developed in chimeric rats or their progeny during observation for over six months.

As a whole, these data show that riPSCs generated by our method can contribute to germline transmission and pose a risk of tumorigenesis lower than that observed using miPSCs generated by a different method.

Generation of interspecific chimeras between mouse and rat with contribution to germline chimerism

We have recently reported successful generation of rat-mouse interspecific chimeras by injection of riPSCs into mouse blastocyst [23]. To assess if the riPSC clones T1-3 or T3-11 can contributed to embryonic development with chimeric formation in wild type

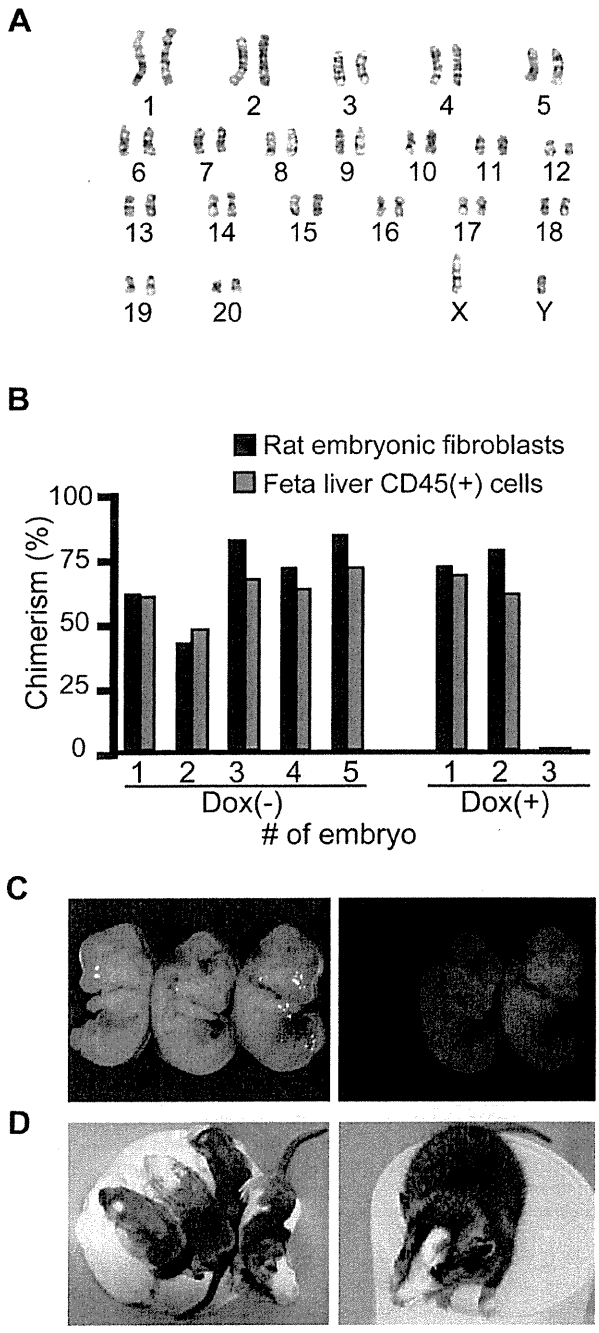

Figure 3. Generation of chimeric rat derived from rat iPS cells. (A) Cytogenetic analysis, riPSCs; G-band staining. Representative data (WI riPSC clone T3-11, passage 7) indicate a chromosomal number of 42, including an XY gender chromosome. (B) Efficiency of chimera rat generation in culture, with or without doxycycline. (C)–(D) Generation of chimeric rat. (C) Analysis of E15.5 material derived from WI riPSCs injected into WI blastocysts. EGFP indicates riPSC-derived cells. (D) Chimeric rats derived from DA riPSCs injected into WI blastocysts. Brown coat color indicates derivation from DA riPSCs. One-week-old pups; left pup (white) not chimeric (left panel). Three-month-old chimeric rat; eye color also is brown (right panel).
doi:10.1371/journal.pone.0022008.g003

mice, we generated rat-mouse interspecific chimeras and analyzed the expression of EGFP in embryonic fibroblasts (Fig. 5A). Embryos derived from both riPSC clones expressed EGFP, indicating that most riPSC clones can form chimeras (Fig. 5B). Moreover, immunostaining found MVH and EGFP double positive cells in testis from interspecific chimeras (n = 2) derived from riPSCs T1-3 (Fig. 5C). These data provide conclusive evidence that these riPSCs are pluripotent and that they can contribute to both interspecific chimera formation and germline transmission.

Discussion

We here show that infection with a lentiviral vector carrying three mouse reprogramming factors (*Oct4*, *Klf4*, and *Sox2*) and culture in the presence of two kinds of kinase inhibitors (MEK inhibitor and GSK3 inhibitor) permit efficient establishment and maintenance of riPSCs from REFs. Established riPSCs possess all the key features of rESCs, such as expression of pluripotency markers Oct4, Nanog, and E-ras, long-term self-renewal, the capacity to differentiate into derivatives of all three germ layers, and, most importantly, the ability to produce chimerism with high efficiency and to contribute to transmission through the germline.

MiPSCs generated by introducing four reprogramming factors (*Oct3/4*, *Sox2*, *Klf4*, and *c-Myc*) are able to produce germline-competent chimeras.

However, a drawback in this four-factor system is reactivation of the c-Myc retrovirus, which increases tumorigenicity in chimeric mice and their progeny. On the other hand, no tumors were observed in mice derived from iPSCs generated by introducing three factors (*Oct3/4*, *Sox2*, and *Klf4*) [27]. Therefore, we used three factors (*Oct3/4*, *Klf4*, and *Sox2*), eliminating c-Myc, with a special emphasis on escape from tumor development. As expected, we observed no tumorigenesis in chimeric rats or their progeny, with monitoring for over six months.

Two main factors can be conceived to affect the successful generation of germline chimeras. One is the conditions under which riPSCs are generated and cultured. In recent studies by Ping Li et al., rESCs were generated using serum-free N2B27 medium containing mLIF and a combination of two or three kinase inhibitors (2i/3i) [19] [20]. RiPSCs also have been generated using knockout DMEM medium containing knockout serum replacement (KSR), 2i, A83-01 and mLIF [16]. Because successful germline transmission was reported only in the rESCs study, we generated riPSCs using N2B27 medium and the 2i/3i culture method. The other is the interaction between iPSC strain and host blastocyst strain. In this study, high efficiency of germline transmission was achieved by injection of WI riPSCs into WI blastocysts (donor cell : host blastocyst combination WI : WI) and of DA riPSCs into WI blastocysts (DA : WI). Other studies have generated rESC germline chimeras in the combinations DA : F344 [16,19], WI :WI and DA/WI [28], and WI-LEA : WI, WI : WI, WI : LEA, and LEA : WI [29]. So far, only a few combinations of iPSCs strains and blastocyst strains have successfully generated germline chimeras. Although we could not obtain offspring from DA riPSCs, we may need to test different strains of blastocysts for more efficient germline transmission.

As in our previous report of interspecific chimeras [23], the riPSCs generated in this study were able to contribute interspecifically to chimera generation and interspecifically to germ cell lineages, indicating that these riPSCs were highly reprogrammed.

Taken together, our results demonstrate that rat somatic cells can be reprogrammed to ground state with germ line competence by transduction of only three reprogramming factors (*Oct3/4*, *Klf4*,

Table 1. Chimera rat generation from rat iPS cells.

Cell line	Wistar T1-3 42XY	Wistar T1-3 42XY	Wistar T1-3 42XY	Wistar T1-3 42XY	Wistar T3-11 42XY	DA T4-27 42XY	DA T4-30 42XY
Passage number	P20	P14	P14	P14	P15	P7	P8
Dox added	(−)	(−)	(+)	(−)	(−)	(−)	(−)
Host blastcyst	WI×DA	WI×WI	WI×WI	WI×WI	WI×WI	WI×WI	WI×WI
Number of Blastcysts injected	43	13	12	39	33	28	42
Developed to fetus	N/A	5 (38%)	3 (25%)	N/A	N/A	N/A	N/A
Developed to pups	4 (9%)	N/A	N/A	18 (46%)	13 (40%)	6 (21%)	26 (62%)
Number of chimeras	2 (50%) 1M,1F	5 (100%)	2 (66%)	11 (61%) 4M, 7F	7 (54%)4M, 3F	2 (33%) 1M, 1F	15*[1] (58%) 7M, 7F
Number of germline chimeras	N/A	N/A	N/A	2/3 M	1/4 M	0/1 M	2/5 M

N/A: not applicable.
*1: One chimera died before weaning.
doi:10.1371/journal.pone.0022008.t001

and *Sox2*). We believe that these riPSCs will open a new area of studies using the rat as a useful animal model.

Materials and Methods

Cell culture

Rat embryonic fibroblasts (REFs) were derived from embryonic day (E)14.5 or E15.5 Wistar (WI) and Dark agouti (DA) rat embryos. WI and DA rats were purchased from Japan SLC (Shizuoka, Japan). REFs were cultured in Dulbecco's modified Eagle's medium (DMEM; Sigma, St. Louis, MO) supplemented with 10% fetal bovine serum (FBS; Hana-Nesco Bio, Moregate BioTech, Australia), 1% L-glutamine penicillin streptomycin (Sigma, St. Louis, MO). Rat iPS cells (riPSCs) were maintained on mitomycin-c treated mouse embryonic fibroblasts (MEFs) in N2B27 medium (Invitrogen, Carlsbad, CA) [30] supplemented with 1,000 U/ml of rat leukemia inhibitory factor (LIF, ESGRO Millipore, Bedford, MA), 3 μM of GSK3 inhibitor CHIR99021 (Axon Medchem BV, Groeningen, The Netherlands), and 1 μM of MEK inhibitor PD0325901 (Stemgent, Cambridge, MA), with or without FGF receptor inhibitor SU5402 (2 μM; Calbiochem, La Jolla, CA). RiPSCs were trypsinized (0.05% trypsin-EDTA: Sigma, St. Louis, MO) into single cells and plated into new wells with a MEFs feeder every 3 or 4 days. Rat embryonic stem cells (rESCs) were maintained as described protocol [28].

Lentiviral vector; generation of riPSCs

The cDNAs of mouse *Oct3/4*, *Sox2*, and *Klf4* were inserted into a doxycycline-inducible system lentiviral vector that also included *EGFP* inserted downstream from a Ubiquitin-C promoter.

To establish riPSCs, Wistar and DA REFs were transduced with this lentiviral vector. Two days later, transduced cells were trypsinized and split among MEFs feeder wells. Eight days later (day 10 after transduction), generated colonies were picked up and mechanically dissociated. Dissociated cells (riPSCs) were plated into new wells with a MEFs feeder (96-well plates). The riPSCs uniformly expressed EGFP under the control of the Ubiquitin-C promoter.

Blastocyst injection and generation of chimeric rats

Chimeric rats were generated by a conventional method: RiPSCs were microinjected into day 4.5 blastocysts of WI×DA-F1 or WI female rats, followed by transfer into host uteri as described. The resultant chimeric rats were mated with WI rats to obtain their progeny [23] [28].

For generation of interspecific chimeras between mouse and rat, we employed conventional method of chimeric mice generation [31]. RiPSCs were microinjected into day 3.5 blastocysts of C57BL/6 or ICR female mice (purchased from SLC Japan), followed by transfer into host uteri as described [23].

ALP staining and immunostaining

Histochemical ALP assays were conducted with Vector Red Alkaline Phosphatase Substrate Kit I (Vector Laboratories, Burlingame, CA) according to the manufacturer's instructions.

For immunofluorescence assays, cells were fixed in 4% paraformaldehyde for 10 min and washed twice with PBS. The fixed cells were incubated in MAXblocking medium (Active Motif, Carlsbad, CA) for 30 min at room temperature (RT) for blocking. The cells were then incubated with primary antibody for one hour at RT in blocking buffer. Cells were then washed with PBS and incubated with secondary antibody in PBS for 30 min at RT. Thereafter the cells were washed with PBS and 4′,6 -diamidino-2-phenylindole (DAPI) was added for nuclear staining.

Primary antibodies used were rabbit anti-mouse Oct3/4 antibody (Bioworld Technology, Minneapolis, MN, 1:100) and rabbit anti-mouse Nanog antibody (ReproCELL, Kanagawa, Japan, 1:100). Secondary antibodies were Alexa Fluor 546 conjugated goat anti-rabbit IgG antibody (1:300) or Alexa Fluor 546 conjugated goat anti-mouse IgG antibody (1:300) (Invitrogen, Carlsbad, CA, 1:300).

Testes were fixed in 4% paraformaldehyde and PBS+sucrose solutions ranging from 10% to 30% (w/v) sucrose before freezing in optimal cutting temperature medium (Tissue Tek, Sakura Finetek, Torrance, CA) and cryostat sectioning. Fixed sections were incubated in MAXblocking medium for 30 min at RT for blocking. Each section was incubated with primary antibody for 1 hr at RT and with secondary antibody for 1 hr at RT. Primary antibodies used were goat anti-GFP (Abcam, Cambridge, MA, 1:100) and rabbit anti-DDX4/MVH (as a primitive germ cell marker; Abcam, 1:100). Secondary antibodies were Alexa Fluor 546 conjugated donkey anti-rabbit IgG antibody and Alexa Fluor 488 conjugated donkey anti-goat IgG antibody (Invitrogen, 1:300). After antibody treatment, sections were mounted with Vectashield (Vector Laboratories), a mounting medium containing DAPI for nuclear counterstaining, and sections were observed under fluorescence microscopy.

Genomic PCR and RT-PCR

Genomic DNA was extracted using QIAamp DNA Mini Kits (Qiagen, Germantown, MD) or the phenol-chloroform method.

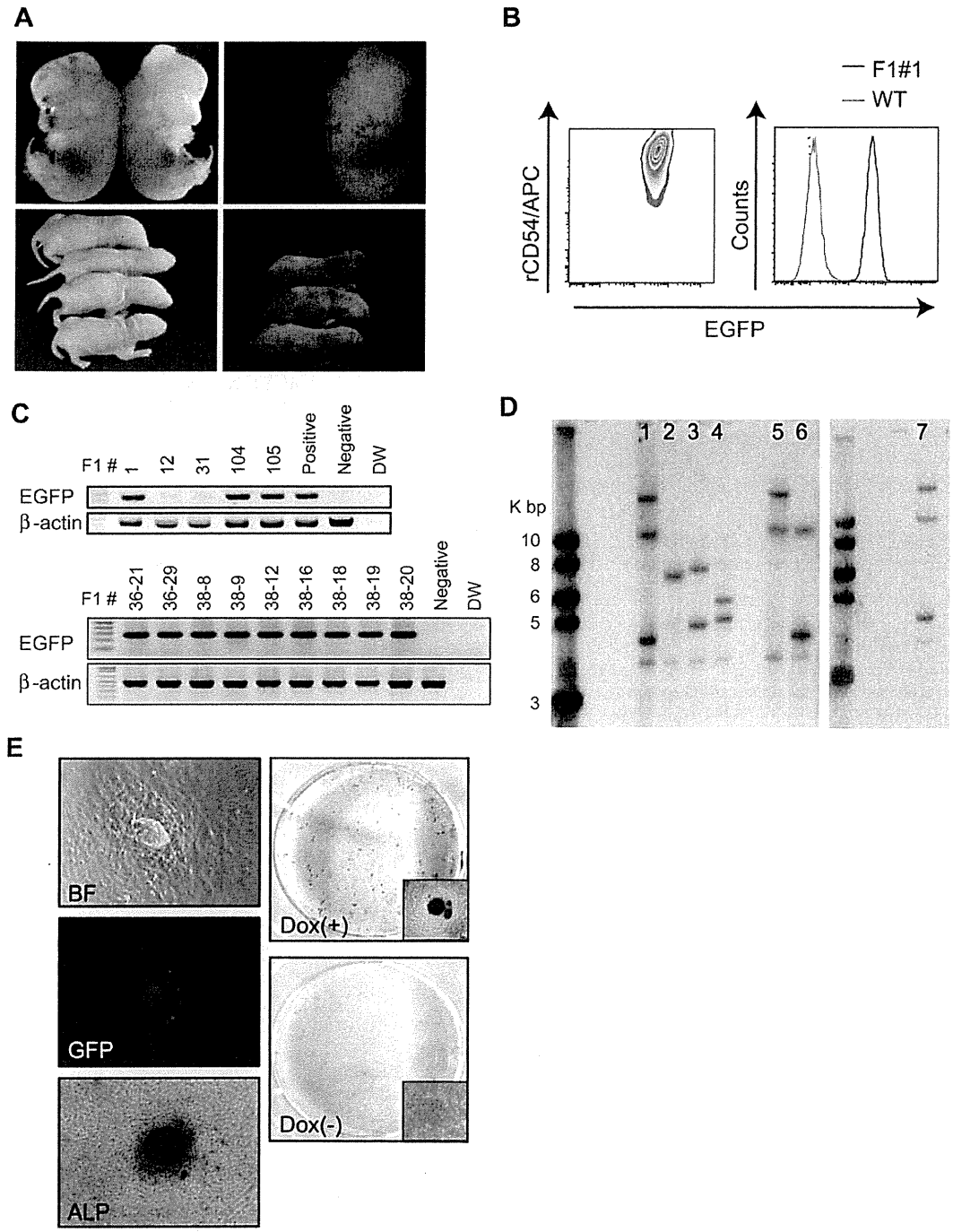

Figure 4. Germline transmission of riPSCs. (A) EGFP of offspring (E15.5; neonate) of chimeric rats. (B) FACS analysis of rat embryonic fibroblasts (REFs) established from F1 rats. (C) Genomic PCR, F1 rats. Some F1 rats harbored *EGFP*. Genomic DNA was obtained from F1 REFs or from tail. (D) Provirus copy numbers determined by Southern blot analysis. Lane1: WI riPSCs, clone T1-3; 2: WI riPSCs, clone T3-11; 3: DA riPSCs, clone T4-27; 4: DA riPSCs, clone T4-30; 5–7: EGFP-expressing F1 rats. (E) REFs established from F1 rats using Dox were reprogrammable: Re-generated riPSCs expressed EGFP and ALP.
doi:10.1371/journal.pone.0022008.g004

PCR was performed in Takara PCR Thermal Cycler Dice® (Takara Bio, Shiga, Japan). Total RNA prepared using the RNAeasy kit (Qiagen) was used as a template for reverse transcription-polymerase chain reaction III (RT-PCR). For genomic PCR and RT-PCR of GFP and β-actin, EX Taq HS (Takara) was used under the following conditions: 94°C for 1 min, followed by 30 or 35 cycles of 94°C for 30 sec, annealing temperature (from 50°C to 62°C) for 30 sec (for genomic PCR) or 1 min (for RT PCR), and 72°C for 30 sec, with a final extension at 72°C for 7 min. PCR products were visualized with

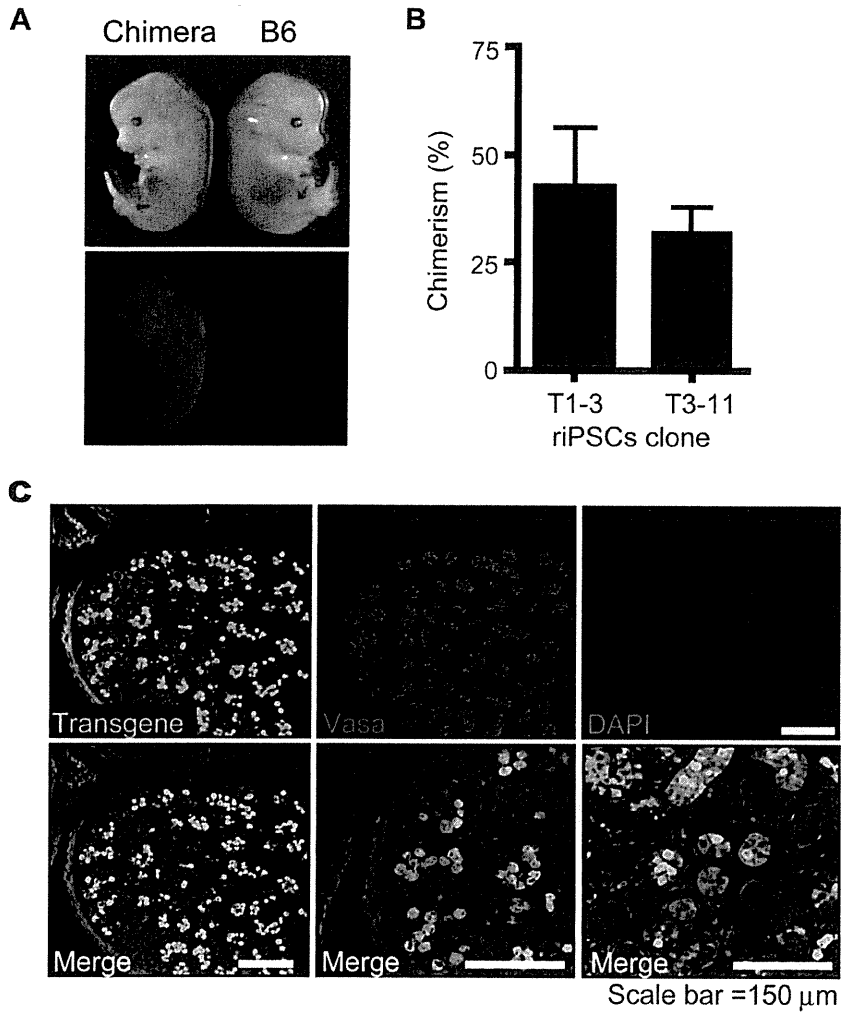

Figure 5. Generation of interspecific chimeras between mouse and rat. (A) RiPSCs injected into mouse blastocysts; analysis, E13.5. EGFP of chimeric mouse (E13.5) generated using rat iPSCs. (B) EGFP (%) of chimerism was shown by FACS analysis of chimeric mouse embryonic fibroblasts (MEFs/REFs) established from F1 rats. (C) Immunostaining of chimeric rats. HMV/DTT (Alexa546) or EGFP fluorescence was observed in testis. EGFP was derived from riPSCs.
doi:10.1371/journal.pone.0022008.g005

ethidium bromide on a 1.2% agarose gel. The primer sequences are listed in Table S2 with annealing temperature and PCR product size.

Southern blotting

High-molecular-weight DNA was obtained from riPSCs or generated REFs. Genomic DNA was digested with XbaI, electrophoresed (1% agarose gel), transferred to a nylon membrane (Hybond-XL: Amersham Biosciences GE Healthcare, UK), and hybridized to [α-^{32}P]dCTP (deoxycytidine 50-triphosphate)-labeled rtTA sequence which is encoded in doxycyclin inducible lentivirus vector.

As the restriction enzyme XbaI cut the vector at one site, the number of fragments hybridized with the probe is considered to be the number of provirus copies integrated into the host genome. Hybridization signals were detected with an auto image analyzer (FLA 5100, Fuji Film, Tokyo, Japan) after exposure to an imaging plate.

Bisulfite sequencing

Genomic DNA was extracted with a genomic DNA purification kit (QIAGEN).

200 ng of genomic DNA from each sample was treated with a Methylamp DNA modification sample kit (Epigentek, Brooklyn, NY) to convert the unmethylated cytosine to uracil according to the manufacturer's instructions. The promoter region of *Oct4* was amplified by PCR using EX Taq HS (Takara), cloned into the pCR 2.1 vector (Invitrogen), and sequenced with M13 reverse and forward primers. PCR primers are listed in Table S2.

Karyotype analysis

Karyotype analysis was performed with standard methods (Nihon Gene Research Laboratories, Miyagi, Japan).

Teratoma formation

A suspension of 0.5~1.0×10^6 single cells was injected intratestis into each testis of 6- to 10-week-old non-obese diabetic/

severe combined immune deficient mice. After 4–8 weeks, tumors were harvested and processed for hematoxylin/eosin staining.

Cell surface analysis

To detect chimerism, REFs and fetal liver cells from riPSC-derived chimeric rats and offspring (E14.5–15.5) were stained with phycoerythrin (PE) - conjugated mouse anti-rat CD45 antibody (OX-1, Biolegend), biotin-conjugated mouse anti-rat CD54 antibody (ICAM-1, 1A29, BD Biosciences PharMingen, San Diego, CA) and Alexa Fluor 647-conjugated goat anti-mouse IgG antibody (BD Biosciences PharMingen). Peripheral blood cells were also stained with PE-conjugated mouse anti-rat CD45 antibody. All stained cells were analyzed by cytometry using FACSCanto II (BD Bioscience).

All experiments were performed under institutional guidelines.

Animal experiments were performed with approval of the Institutional Animal Care and Use Committee of the Institute of Medical Science, University of Tokyo (permit numbers: A09-29, A09-30, A10-23) and the Institutional Animal Care and Use Committee of the National Institute for Physiological Sciences (permit number: 11A022).

Supporting Information

Figure S1 Karyotype analysis of cells cultured with 3i. Cytogenetic analysis, riPSCs; G-band staining. Representative data of WI riPSCs, clone T1-3, at passage 20 when cultured with 3i-medium indicate trisomy of chromosome 9 in 2 out of 50 cells, including an XY gender chromosome, but within normal range of polyploidy. A few cells exhibiting trisomy of chromosome 9 in another two clones were cultured with 3i-medium.
(TIF)

Figure S2 Phenotype of chimeric rat derived from DA riPSCs, clone T4-30. (A) EGFP expression in testis. (B) Immunostaining of chimeric rat testis. HMV/DTT (Alexa546) or EGFP fluorescence was observed in testis. EGFP was derived from riPSCs.
(TIF)

Table S1 Summary of offspring-rat generation from riPSCs.
(DOC)

Table S2 Summary of primer sequences.
(DOCX)

Acknowledgments

We thank Y. Yamazaki for excellent technical support, Dr. Takayama for excellent technical advice, Dr. Eto for critical advice of preparing the manuscript, and Dr. A. S. Knisely for critical reading of the paper.

Author Contributions

Conceived and designed the experiments: SH TY HN. Performed the experiments: SH TY MH MK-I MS TK AU HS YW. Analyzed the data: SH TK SY. Contributed reagents/materials/analysis tools: TY MA. Wrote the paper: SH TY. Final approval of the manuscript: TY HN.

References

1. Evans MJ, Kaufman MH (1981) Establishment in culture of pluripotential cells from mouse embryos. Nature 292: 154–156.
2. Takahashi K, Yamanaka S (2006) Induction of pluripotent stem cells from mouse embryonic and adult fibroblast cultures by defined factors. Cell 126: 663–676.
3. Okita K, Ichisaka T, Yamanaka S (2007) Generation of germline-competent induced pluripotent stem cells. Nature 448: 313–317.
4. Vassilieva S, Guan K, Pich U, Wobus AM (2000) Establishment of SSEA-1- and Oct-4-expressing rat embryonic stem-like cell lines and effects of cytokines of the IL-6 family on clonal growth. Exp Cell Res 258: 361–373.
5. Buehr M, Nichols J, Stenhouse F, Mountford P, Greenhalgh CJ, et al. (2003) Rapid loss of Oct-4 and pluripotency in cultured rodent blastocysts and derivative cell lines. Biol Reprod 68: 222–229.
6. Demers SP, Yoo JG, Lian L, Therrien J, Smith LC (2007) Rat embryonic stem-like (ES-like) cells can contribute to extraembryonic tissues in vivo. Cloning Stem Cells 9: 512–522.
7. Ueda S, Kawamata M, Teratani T, Shimizu T, Tamai Y, et al. (2008) Establishment of rat embryonic stem cells and making of chimera rats. PLoS One 3: e2800.
8. Honda A, Hirose M, Inoue K, Ogonuki N, Miki H, et al. (2008) Stable embryonic stem cell lines in rabbits: potential small animal models for human research. Reprod Biomed Online 17: 706–715.
9. Honda A, Hirose M, Hatori M, Matoba S, Miyoshi H, et al. (2010) Generation of induced pluripotent stem cells in rabbits: potential experimental models for human regenerative medicine. J Biol Chem 285: 31362–31369.
10. Esteban MA, Xu J, Yang J, Peng M, Qin D, et al. (2009) Generation of induced pluripotent stem cell lines from Tibetan miniature pig. J Biol Chem 284: 17634–17640.
11. Ezashi T, Telugu BP, Alexenko AP, Sachdev S, Sinha S, et al. (2009) Derivation of induced pluripotent stem cells from pig somatic cells. Proc Natl Acad Sci U S A 106: 10993–10998.
12. Liu H, Zhu F, Yong J, Zhang P, Hou P, et al. (2008) Generation of induced pluripotent stem cells from adult rhesus monkey fibroblasts. Cell Stem Cell 3: 587–590.
13. Tomioka I, Maeda T, Shimada H, Kawai K, Okada Y, et al. (2010) Generating induced pluripotent stem cells from common marmoset (Callithrix jacchus) fetal liver cells using defined factors, including Lin28. Genes Cells 15: 959–969.
14. Wu Y, Zhang Y, Mishra A, Tardif SD, Hornsby PJ (2010) Generation of induced pluripotent stem cells from newborn marmoset skin fibroblasts. Stem Cell Res 4: 180–188.
15. Takahashi K, Tanabe K, Ohnuki M, Narita M, Ichisaka T, et al. (2007) Induction of pluripotent stem cells from adult human fibroblasts by defined factors. Cell 131: 861–872.
16. Li W, Wei W, Zhu S, Zhu J, Shi Y, et al. (2009) Generation of rat and human induced pluripotent stem cells by combining genetic reprogramming and chemical inhibitors. Cell Stem Cell 4: 16–19.
17. Takayama N, Nishimura S, Nakamura S, Shimizu T, Ohnishi R, et al. (2010) Transient activation of c-MYC expression is critical for efficient platelet generation from human induced pluripotent stem cells. J Exp Med 207: 2817–2830.
18. Ying QL, Wray J, Nichols J, Batlle-Morera L, Doble B, et al. (2008) The ground state of embryonic stem cell self-renewal. Nature 453: 519–523.
19. Li P, Tong C, Mehrian-Shai R, Jia L, Wu N, et al. (2008) Germline competent embryonic stem cells derived from rat blastocysts. Cell 135: 1299–1310.
20. Buehr M, Meek S, Blair K, Yang J, Ure J, et al. (2008) Capture of authentic embryonic stem cells from rat blastocysts. Cell 135: 1287–1298.
21. Liao J, Cui C, Chen S, Ren J, Chen J, et al. (2009) Generation of induced pluripotent stem cell lines from adult rat cells. Cell Stem Cell 4: 11–15.
22. Chang MY, Kim D, Kim CH, Kang HC, Yang E, et al. (2010) Direct reprogramming of rat neural precursor cells and fibroblasts into pluripotent stem cells. PLoS One 5: e9838.
23. Kobayashi T, Yamaguchi T, Hamanaka S, Kato-Itoh M, Yamazaki Y, et al. (2010) Generation of rat pancreas in mouse by interspecific blastocyst injection of pluripotent stem cells. Cell 142: 787–799.
24. Mitsui K, Tokuzawa Y, Itoh H, Segawa K, Murakami M, et al. (2003) The homeoprotein Nanog is required for maintenance of pluripotency in mouse epiblast and ES cells. Cell 113: 631–642.
25. Loh YH, Wu Q, Chew JL, Vega VB, Zhang W, et al. (2006) The Oct4 and Nanog transcription network regulates pluripotency in mouse embryonic stem cells. Nat Genet 38: 431–440.
26. Meissner A, Mikkelsen TS, Gu H, Wernig M, Hanna J, et al. (2008) Genome-scale DNA methylation maps of pluripotent and differentiated cells. Nature 454: 766–770.
27. Nakagawa M, Koyanagi M, Tanabe K, Takahashi K, Ichisaka T, et al. (2008) Generation of induced pluripotent stem cells without Myc from mouse and human fibroblasts. Nat Biotechnol 26: 101–106.
28. Hirabayashi M, Kato M, Kobayashi T, Sanbo M, Yagi T, et al. (2010) Establishment of rat embryonic stem cell lines that can participate in germline chimerae at high efficiency. Mol Reprod Dev 77: 94.
29. Kawamata M, Ochiya T (2010) Generation of genetically modified rats from embryonic stem cells. Proc Natl Acad Sci U S A 107: 14223–14228.
30. Ying QL, Stavridis M, Griffiths D, Li M, Smith A (2003) Conversion of embryonic stem cells into neuroectodermal precursors in adherent monoculture. Nat Biotechnol 21: 183–186.
31. Nagy A (2003) Manipulating the mouse Embryo: A laboratory manual. Cold Sprimg Harbor, NY: Cold Spring Harbor Laboratory Press.

THE JOURNAL OF BIOLOGICAL CHEMISTRY VOL. 286, NO. 6, pp. 4760–4771, February 11, 2011

Development of Defective and Persistent Sendai Virus Vector

A UNIQUE GENE DELIVERY/EXPRESSION SYSTEM IDEAL FOR CELL REPROGRAMMING[*S]

Received for publication, September 9, 2010, and in revised form, December 5, 2010 Published, JBC Papers in Press, December 7, 2010, DOI 10.1074/jbc.M110.183780

Ken Nishimura,[a,b] Masayuki Sano,[a] Manami Ohtaka,[a,c] Birei Furuta,[d] Yoko Umemura,[a] Yoshiro Nakajima,[a] Yuzuru Ikehara,[e] Toshihiro Kobayashi,[f,g] Hiroaki Segawa,[h1] Satoko Takayasu,[a,c] Hideyuki Sato,[f,g] Kaori Motomura,[a,c] Eriko Uchida,[i] Toshie Kanayasu-Toyoda,[d] Makoto Asashima,[a,j] Hiromitsu Nakauchi,[f,g] Teruhide Yamaguchi,[d] and Mahito Nakanishi[a2]

From the [a]Research Center for Stem Cell Engineering, [e]Research Center for Medical Glycoscience, and [h]Organ Development Research Laboratory, National Institute of Advanced Industrial Science and Technology (AIST), 1-1-1 Higashi, Central 4, Tsukuba, Ibaraki 305-8562, [b]PRESTO, Japan Science and Technology Agency, 4-1-8 Hon-cho, Kawaguchi, Saitama 332-0012, [c]Japan Biological Informatics Consortium, TIME24 Building, 2-4-32 Aomi, Koto-ku, Tokyo 135-8073, [d]Division of Biological Chemistry and Biologicals and [i]Division of Cellular and Gene Therapy Products, National Institute of Health Sciences, 1-18-1 Kami-Yoga, Setagaya-ku, Tokyo 158-8501, [f]Division of Stem Cell Therapy, Center for Stem Cell Biology and Regenerative Medicine, the Institute of Medical Science, the University of Tokyo, and the [g]Nakauchi Stem Cell and Organ Regeneration Project, ERATO, Japan Science and Technology Agency, 4-6-1 Shirokane-dai, Minato-ku, Tokyo 108-8639, and the [j]Department of Life Sciences (Biology), Graduate School of Arts and Sciences, The University of Tokyo, 3-8-1 Komaba, Meguro-ku, Tokyo 153-8902, Japan

The ectopic expression of transcription factors can reprogram differentiated tissue cells into induced pluripotent stem cells. However, this is a slow and inefficient process, depending on the simultaneous delivery of multiple genes encoding essential reprogramming factors and on their sustained expression in target cells. Moreover, once cell reprogramming is accomplished, these exogenous reprogramming factors should be replaced with their endogenous counterparts for establishing autoregulated pluripotency. Complete and designed removal of the exogenous genes from the reprogrammed cells would be an ideal option for satisfying this latter requisite as well as for minimizing the risk of malignant cell transformation. However, no single gene delivery/expression system has ever been equipped with these contradictory characteristics. Here we report the development of a novel replication-defective and persistent Sendai virus (SeVdp) vector based on a noncytopathic variant virus, which fulfills all of these requirements for cell reprogramming. The SeVdp vector could accommodate up to four exogenous genes, deliver them efficiently into various mammalian cells (including primary tissue cells and human hematopoietic stem cells) and express them stably in the cytoplasm at a prefixed balance. Furthermore, interfering with viral transcription/replication using siRNA could erase the genomic RNA of SeVdp vector from the target cells quickly and thoroughly. A SeVdp vector installed with *Oct4/Sox2/Klf4/c-Myc* could reprogram mouse primary fibroblasts quite efficiently; ~1% of the cells were reprogrammed to Nanog-positive induced pluripotent stem cells without chromosomal gene integration. Thus, this SeVdp vector has potential as a tool for advanced cell reprogramming and for stem cell research.

The generation of induced pluripotent stem (iPS)[3] cells by reprogramming tissue cells with defined factors opened the door for realizing the medical application of patient-derived engineered stem cells (1). iPS cells were established originally by the ectopic expression of multiple transcription factors (*e.g.* Oct3/4, Sox2, Klf4, and c-Myc) using a retroviral vector (1). Since then, researchers have established iPS cells by several different approaches (and by their combination), including gene transfer, protein transduction, and treatment with chemical compounds (2). However, because of superior reproducibility and efficacy, ectopic expression of reprogramming factors by gene transfer is still the primary method of choice.

Various lines of evidence indicate that efficient cell reprogramming requires the sustained and simultaneous expression of several (usually 4) exogenous factors for at least 10–20 days (3). On the other hand, after reprogramming has been completed, these exogenous factors should be replaced promptly with their endogenous counterparts if the cells are to acquire autoregulated pluripotency (3). For this reason, retroviral and lentiviral vectors have been used preferentially; chromosomal insertion of the vector genome allows for stable gene expression, whereas epigenetic modification of the viral promoter shuts off the vector-mediated gene expression after cell reprogramming has been accomplished. Nevertheless, cell reprogramming with these insertional vectors has a crucial disadvantage in that silencing and reactivation of the inte-

* This work was supported in part by a grant from the New Energy and Industrial Technology Development Organization of Japan, by the Program for Promotion of Fundamental Studies in Health Sciences of the National Institute of Biomedical Innovation, and by JST PRESTO Program.
[S] The on-line version of this article (available at http://www.jbc.org) contains supplemental Tables S1 and S2 and Figs. S1–S4.
[1] Present address: Fuji-Gotemba Research Laboratories, Chugai Pharmaceutical Co. Ltd., 1-135, Komakado, Gotemba, Shizuoka, 412-8513, Japan.
[2] To whom correspondence should be addressed. Tel.: 81-29-861-3040; Fax: 81-29-861-2798; E-mail: mahito-nakanishi@aist.go.jp.

[3] The abbreviations used are: iPS, induced pluripotent stem; ES, embryonic stem; SeV, Sendai virus; SeVdp, defective and persistent Sendai virus; Bs, blasticidin S; Zeo, zeocin; *Zeo*, phleomycin-binding protein gene; *Bsr*, blasticidin S deaminase gene; *Hyg*, hygromycin B phosphotransferase gene; EGFP, enhanced green fluorescent protein; KO, Kusabira Orange; KR, Keima Red; MEF, mouse embryonic fibroblast; NP, nucleocapsid protein; CFU, colony-forming unit.